

Nucleon resonances in the fourth resonance region

A.V. Anisovich^{1,2}, E. Klempt¹, V.A. Nikonov^{1,2}, A.V. Sarantsev^{1,2}, and U. Thoma¹

¹ Helmholtz-Institut für Strahlen- und Kernphysik, Universität Bonn, Germany

² Petersburg Nuclear Physics Institute, Gatchina, Russia

Received: March 7, 2022/ Revised version:

Abstract. Nucleon and Δ resonances in the fourth resonance region are studied in a multichannel partial-wave analysis which includes nearly all available data on pion- and photo-induced reactions off protons. In the high-mass range, above 1850 MeV, several alternative solutions yield a good description of the data. For these solutions, masses, widths, pole residues and photo-couplings are given. In particular, we find evidence for nucleon resonances with spin-parities $J^P = 1/2^+ \dots 7/2^+$. For one set of solutions, there are four resonances forming naturally a spin-quartet of resonances with orbital angular momentum $L = 2$ and spin $S = 3/2$ coupling to $J = 1/2, \dots, 7/2$. Just below 1.9 GeV we find a spin doublet of resonances with $J^P = 1/2^-$ and $3/2^-$. Since a spin partner with $J^P = 5/2^-$ is missing at this mass, the two resonances form a spin doublet which must have a symmetric orbital-angular-momentum wave function with $L = 1$. For another set of solutions, the four positive-parity resonances are accompanied by mass-degenerate negative-parity partners – as suggested by the conjecture of chiral symmetry restoration. The possibility of a $J^P = 1/2^+, 3/2^+$ spin doublet at 1900 MeV belonging to a 20-plet is discussed.

PACS. 11.80.Et Partial-wave analysis – 11.80.Gw Multichannel scattering – 13.30.-a Decays of baryons – 13.30.Ce Leptonic, semileptonic, and radiative decays – 13.30.Eg Hadronic decays – 13.60.Le Meson production – 14.20.Gk Baryon resonances (S=C=B=0)

1 Introduction

One of the most striking successes of the quark model was the successful calculation of the spectrum and of the mixing angles of low-lying excited baryons, using a harmonic oscillator potential and a hyperfine interaction as derived from first-order perturbative QCD [1, 2, 3]. In the course of time, the model was improved by taking into account relativistic corrections [4] or by fully relativistic calculations [5]. The effective one-gluon exchange interaction [1, 2, 3, 4] was replaced by one-boson exchange interactions between constituent quarks [6] or by instanton-induced interactions [5]. The improved baryon wave functions provided the basis for calculations of partial decay widths [7, 8, 9, 10, 11], of helicity amplitudes [12, 13], and of form factors [14, 15, 16, 17]. The spectrum of nucleon and Δ resonances calculated on the lattice [18] shows striking agreement with expectations based on quark models: with increasing mass, there are alternating clusters of states with positive and with negative parity. No parity doubling is observed, and the number of expected states on the lattice and in quark models seems to be the same. In spite of these considerable successes, there are still many open questions in baryon spectroscopy (for reviews, see [19, 20, 21]) which need further investigations.

i. There are some low-mass baryon resonances which resist a straightforward interpretation as quark model states. In effective field theories of strong interactions, these resonances can be generated dynamically from meson-baryon interactions. Well-known examples are the Roper resonance $N_{1/2}^+(1440)$ [22],

the $N_{1/2}^-(1535)$ [23], and the $\Lambda_{1/2}^-(1405)$ [24]. The relation between quark-model states and those dynamically generated is not yet explored.

ii. There is the problem of the *missing resonances*: quark models predict many more resonances than have been observed so far, especially at higher energies. This problem is aggravated by the prediction of additional states, hybrid baryons, in which the gluonic string mediating the interaction between the quarks is itself excited [25]. Their spectrum is calculated to intrude the spectrum of baryon resonances at 2 GeV and above.

iii. Baryon excitations come very often in parity doublets, of pairs of resonances having opposite parity but similar masses. The occurrence of parity doublets is unexpected in quark models. It has led to the conjecture that chiral symmetry could be restored when baryons are excited [26, 27, 28, 29]. It has been suggested that the transition from constituent quarks to current quarks can be followed by precise measurements of the masses of excited hadron resonances [30]. The splitting in (squared) mass between two states forming a parity doublet (like $\Delta(1950)$ F_{17} and $\Delta(2200)G_{17}$, 1.04 GeV^2) is slightly smaller than the mean mass square difference per unit of angular momentum (the string tension, 1.1 GeV^2). This effect can possibly be interpreted as weak attraction between parity partners in the 2 GeV mass region and as onset of a regime in which chiral symmetry is restored [31]. This possibility depends, of course, crucially on the assumption that chiral symmetry is restored in the high-mass part of the hadron excitation spectrum.

iv. A very simple phenomenological two-parameter mass formula [32] describes the baryon mass spectrum with an unexpectedly good precision. The formula can be derived [33] within an analytically solvable “gravitational” theory simulating QCD [34] which is defined in a five-dimensional Anti-de Sitter (AdS) space embedded in six dimensions. The mass formula predicts mass-degenerate spin multiplets with defined orbital angular momentum L in which the orientation of the quark spin S relative to L has no or little impact on the baryon mass, a prediction which needs to be confirmed or rejected by further experimental information.

In this paper, we report properties of nucleon resonances with masses of about 2 GeV, a mass range which is often called 4th resonance region. The resonance regions are well seen in Fig. 1a, starting with the $\Delta(1232)$ tail as 1st resonance region followed by peaks, indicating the 2nd, and 3rd and 4th resonance region. The properties of nucleon resonances are determined in a coupled-channel partial wave analysis of a large body of data. The analysis methods are documented in [35, 36, 37, 38], earlier results can be found in [39, 40, 41, 42, 43, 44]. Recently, we have enlarged considerably our data base. In particular both, the recent high-statistics data [45, 46, 47, 48, 49, 50, 51, 52, 53] on photoproduction of hyperons but also the old low-statistics data on pion-induced hyperon production [54, 55, 56, 57, 58] proved to be very sensitive to properties of contributing resonances. In the first paper [59], we reported evidence for $N(1710)P_{11}$, $N(1875)P_{11}$, $N(1900)P_{13}$, $\Delta(1910)P_{31}$, $\Delta(1600)P_{33}$ and $\Delta(1920)P_{33}$. The main aim was to investigate if resonances seen in the Karlsruhe-Helsinki (KH84) [60] and the Carnegie-Mellon (CM) [61] analyses of πN elastic scattering but not observed by the Data Analysis Center at GWU [62] can be identified in inelastic reactions. The positive answer encourages us to study the “full” spectrum of nucleon resonances in the 2 GeV region.

The data on hyperon production with the largest statistics are those with $K\Lambda$ in the final state. These are sensitive to nucleon resonances only. Data on $K\Sigma$ contribute to both, to nucleon and Δ resonances, the statistical errors for data on this channel are considerably higher. For this reason, we concentrate here on nucleon resonances. Δ resonances will be discussed when new high-statistics data on the $\gamma p \rightarrow \pi^0 \pi^0 p$ and $p\pi^0 \eta$ production channels from ELSA are included in our data base.

At present, existence and properties of nucleon resonances are mostly derived from energy dependent fits to the energy-independent partial wave analyses of πN elastic scattering data [60, 61, 62]. Large discrepancies between the results of the three groups reveal the weak points of these analyses: first, the amplitudes cannot be constructed from the data without theoretical input. For a full amplitude reconstruction, the differential cross section $d\sigma/d\Omega$, target asymmetry, and spin rotation parameters need to be known in the entire energy and angular range. Without spin rotation parameters, only the absolute values of the spin-flip and spin non-flip amplitudes $|H|$ and $|G|$ can be determined but not their phases. Dispersion relations must be enforced but, unfortunately, their impact on the partial wave solutions seems not very well defined (judged from the differences in the results obtained by [60, 61, 62]). Second, the inelasticity of the πN amplitude is a free fit parameter to be determined

for every bin. It is unconstrained by the decay modes of resonances. In practice, this freedom can be exploited to fit the elastic partial wave amplitudes with equally acceptable χ^2 using a variety of models with a different content of resonances. In the approach presented here, the inelasticity of the energy independent elastic πN amplitudes are constrained by a large number of data sets on inelastic reactions. The inelasticity of the πN amplitude is no longer a free fit parameter to be determined for every bin. Thresholds, couplings to the different channels, and the opening of new channels are properly taken into account.

We use the naming scheme adopted in [59]. For resonances listed in Review of Particle Properties (RPP) [69] we use the conventional names of the Particle Data Group: $N(\text{mass})L_{2I,2J}$ and $\Delta(\text{mass})L_{2I,2J}$ where I and J are isospin and total spin of the resonance and L the orbital angular momentum in the decay of the resonance into nucleon and pion. For resonances not included in [69], we use $N_{JP}(\text{mass})$ and $\Delta_{JP}(\text{mass})$ which gives the spin-parity of the resonance directly.

2 Data, PWA method, and fits

The coupled-channel partial wave analysis uses the πN elastic amplitudes, alternatively from KH84 [60] or from SAID [62]. SAID results are given with errors; for KH84, no errors are given. We assume $\pm 5\%$ errors for the fits. Data are included on the reactions $\pi^- p \rightarrow \eta n$, $\pi N \rightarrow K\Lambda$, $\pi N \rightarrow K\Sigma$, $\gamma p \rightarrow \pi^0 p$, $\gamma p \rightarrow \pi^+ n$, $\gamma p \rightarrow K\Lambda$, $\gamma p \rightarrow K\Sigma$, $\pi^- p \rightarrow \pi^0 \pi^0 n$, and $\gamma p \rightarrow \pi^0 \pi^0 p$, $\gamma p \rightarrow \pi^0 \eta p$. Measurements of polarization variables, with polarization in the initial or final state or with target polarization, are included in the analysis whenever such data are available. A complete list of the reactions and references to the data is given in Tables 1-5 of reference [59]. The data sets we added here are differential cross section and recoil asymmetry on the $\pi^+ p \rightarrow K^+ \Sigma^+$ reaction in the mass region below 1850 MeV [70, 71, 72, 73, 74], new CLAS data on $\gamma p \rightarrow K^+ \Sigma^0$ [67], new MAMI data on $\gamma p \rightarrow \eta p$ [75] and for the reaction $\gamma p \rightarrow K^0 \Sigma^+$ the differential cross section [68]. We now excluded from the analysis the $\gamma p \rightarrow \eta p$ data on the target asymmetry: since there seems to be an inconsistency between these data and new preliminary CB-ELSA/TAPS data [76].

The MAMI data were well fitted, without need for significant changes in mass, widths or coupling constants of the contributing resonances. In a narrow mass region at about 1700 MeV, statistically significant deviations between data and fit showed up. Dedicated fits were made [77] to study this effect. The fits improved by introduction of a narrow resonance, or by introducing a ωN coupling in the S_{11} wave. Suggestions for experiments were made capable to decide which alternative is realized in nature. For most resonances, the ELSA data set had no noticeable effect on their properties neither. But when these data were introduced in the fit, an additional resonance $N_{3/2-}(1870)$ was needed (which was then also of substantial help in describing other data sets).

The analysis method [35, 36, 37, 38], uses relativistic invariant operators which are constructed directly from the 4-vectors of the particles. Resonances are parameterized in multi-channel

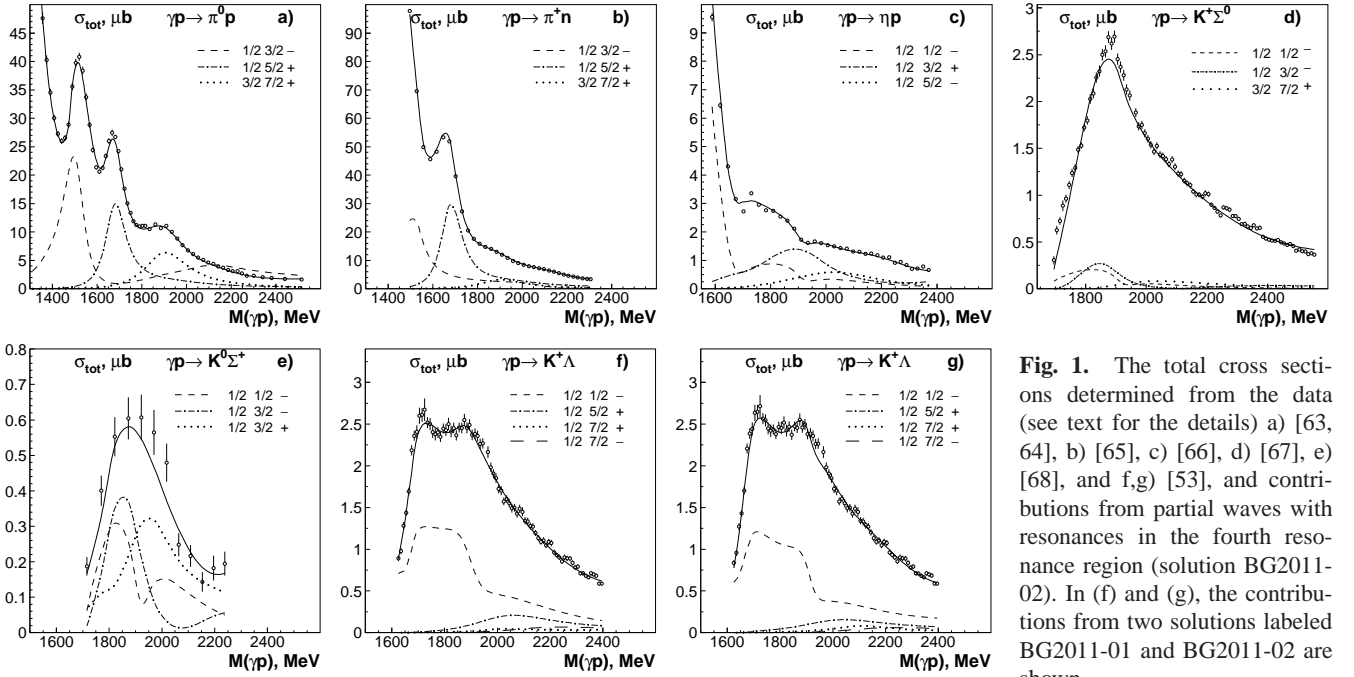


Fig. 1. The total cross sections determined from the data (see text for the details) a) [63, 64], b) [65], c) [66], d) [67], e) [68], and f,g) [53], and contributions from partial waves with resonances in the fourth resonance region (solution BG2011-02). In (f) and (g), the contributions from two solutions labeled BG2011-01 and BG2011-02 are shown.

K matrices. Background terms are partly added within the K-matrix either as constants or in the form $(a + b\sqrt{s})/(s - s_0)$ with s_0 simulating left-hand cuts (s_0 being negative, at a few GeV^2), partly they are added as t -channel meson-exchange or u -channel baryon-exchange amplitude. These amplitudes are sufficiently flexible to describe the data mentioned above with good precision. In the pion induced reactions the t - and u -channel exchanges are projected into the partial waves and contribution from lowest partial waves (up to spin 3/2) are subtracted from the t and u -exchange amplitudes. Thus, for the lowest partial waves, these exchanges are taken effectively into account as K-matrix non-resonant terms. Such approach ensures that we fully satisfy the unitarity condition for the pion induced reactions. We remind the reader that we found two classes of solutions, called BG2010-01 and BG2010-02. In this article, figures are shown for solutions which are called BG2011-01 and BG2011-02 which are modifications of solutions BG2010-01 and BG2010-02 due to including/excluding of the data sets discussed above and including a number of high mass poles into the K-matrix parameterization. Contributions of partial waves with resonances in the fourth resonance region are shown in Fig. 1. The total cross sections are determined by summation over the (binned) experimental differential cross sections, including statistical and systematic errors, and using our partial wave results in the angular range where no data exist. In Figs. 2 to 6 we exemplify the fit quality by showing a few data sets.

As can be seen from the figures, there are only marginal differences in fit quality between the two solutions. Indeed, the overall χ^2 of the two fits hardly differs. Many resonances have very similar properties in both types of solutions but some are distinctively different. Significant differences are found, e.g., in the helicity amplitudes for the production of $N(1710)P_{11}$ and $N(1720)P_{13}$, their $N\eta$ decay fractions [59] and in the masses and widths of a few resonances with low RPP starting. Within both classes of solutions, a large variety of different fits were made, e.g. by adding a further pole in a particular

partial wave or by changing start values of the fit. The spread of results within a class of solutions is used to define the errors. The statistical errors returned by the fit are usually unrealistically small.

In Figs. 5 and 6 we show a few examples, data and fit curves, covering the central part of the fourth resonance region. In addition to the main fit represented by a solid curve we also show fits (dashed curve) in which one of the resonances is removed. These curves are discussed below. The fits are meant to illustrate the significance of a particular data set to resonance formation. Further plots can be seen in [59] and on our web page (<http://pwa.hiskp.uni-bonn.de>).

In the fits to the data, we use weighting factors ω to avoid that low statistics polarization data are overruled by high-statistics data on, e.g., differential cross sections. The weights are adjusted to achieve a visually acceptable fit quality for all data sets. The total χ^2 is then calculated as weighted sum of the χ^2 from the individual data sets: $\sum \omega_i N_i / \sum N_i$ where ω_i and N_i is the weight and number of events in the data set i . To the χ^2 we add the likelihood ($\delta\chi^2 = 2\delta \ln \mathcal{L}$) of the event-based likelihood fit to multi-body final states. The absolute value of the likelihood depends on the normalization and has no meaning. Therefore only differences of the total χ^2 are given.

The fit quality decreases above 2.2 to 2.3 GeV . We did not try to systematically improve the description in this mass region. A large number of resonances is expected, and the data base is certainly not yet sufficient to arrive at solid conclusions.

3 Discussion of partial waves

3.1 Positive parity nucleon resonances

Positive-parity nucleon resonances above the nucleon may belong - in the harmonic oscillator approximation - to the second excitation band. Well known are the Roper resonance $N(1440)$

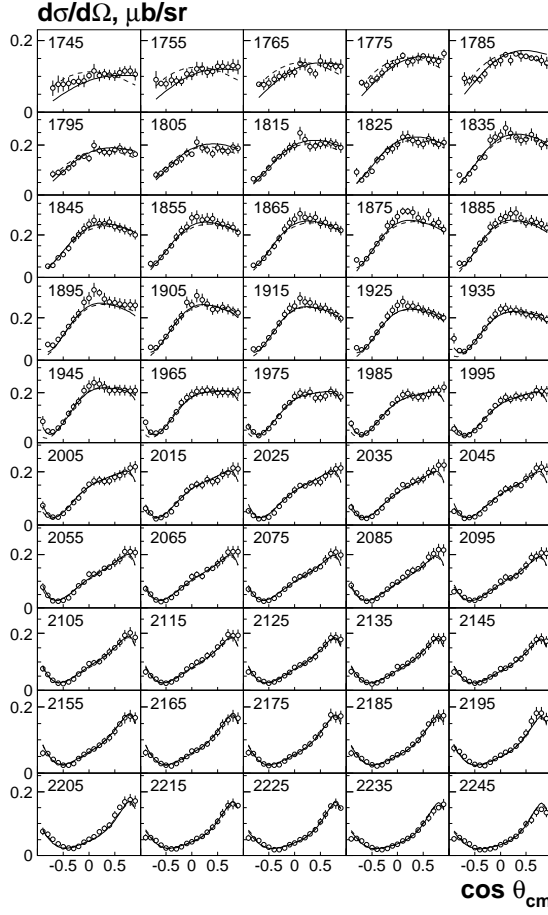


Fig. 2. Differential cross section for $\gamma p \rightarrow K^+ \Sigma^0$ [67]. The full curve corresponds to solution BG2011-02 ($\chi^2=1.44$), the dashed one to BG2011-01 ($\chi^2=1.44$).

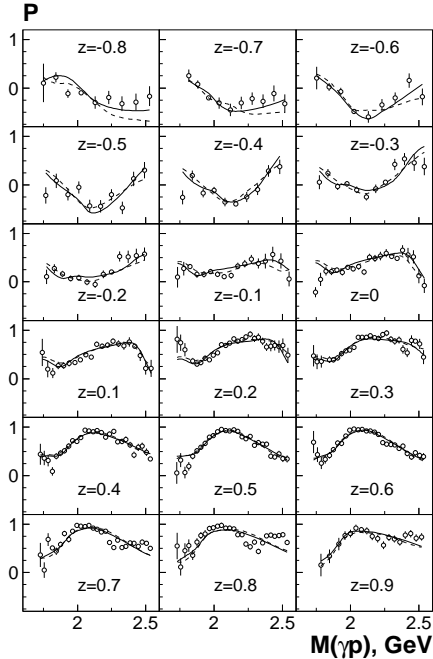


Fig. 3. Recoil polarization for $\gamma p \rightarrow K^+ \Sigma^0$ [67]. The full curve corresponds to solution BG2011-02 ($\chi^2=2.70$), the dashed one to BG2011-01 ($\chi^2=2.76$).

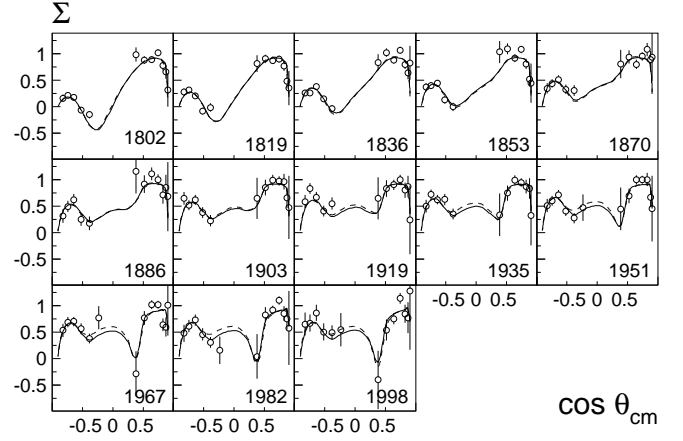


Fig. 4. Beam asymmetry for single- π^0 photoproduction $\gamma p \rightarrow \pi^0 p$ reaction [78]. The full curve corresponds to the solution BG2011-02 and the dashed one corresponds to the solution BG2011-01.

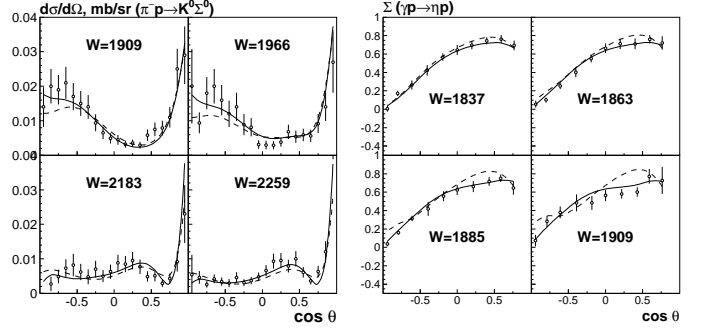


Fig. 5. Left: Differential cross section for $\pi^- p \rightarrow K^0 \Sigma^0$ [57]. Right: Beam asymmetry from GRAAL for $\gamma p \rightarrow \eta p$ [79]. The full curves correspond to the solution BG2011-02, the dashed ones to the best fit without a second $5/2^-$ resonance.

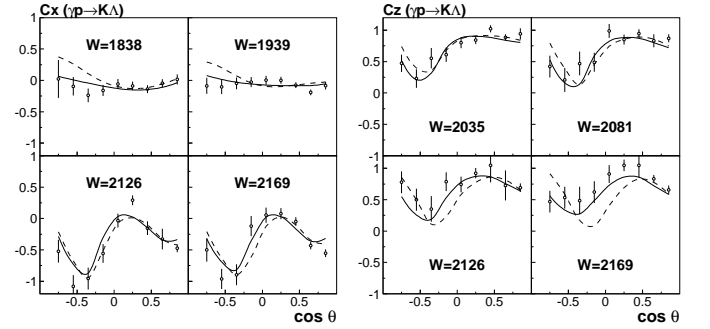


Fig. 6. Polarization transfer variables C_x , C_z from circularly polarized photons to Λ hyperons [49]. The full curves correspond to the solution BG2011-02, the dashed ones to the best fit without a resonant contributions in the nucleon $5/2^+$ partial wave above 1.8 GeV.

P_{11} , the 3-star $N(1710)P_{11}$ (challenged by SAID [62]), and the spin-doublet $N(1720)P_{13}$ and $N(1680)F_{15}$. Above, there is a possible quartet of nucleon resonances,

$$N_{1/2+}(1875), N(1900)P_{13}, N(2000)F_{15}, N(1990)F_{17}.$$

The $I(J^P) = \frac{1}{2}(\frac{1}{2}^+)$ resonance was reported in [59], the other three resonances are listed in RPP with two stars: evidence for their existence is fair. None of them is needed in the SAID anal-

ysis [62]. The next known positive-parity nucleon resonance is the four-star $N(2220)H_{19}$; it should have a spin partner with $I(J^P) = \frac{1}{2}(\frac{7}{2}^+)$. These two resonances belong to fourth excitation band.

3.1.1 $I(J^P) = \frac{1}{2}(\frac{1}{2})^+$ and $\frac{1}{2}(\frac{3}{2})^+$

Nucleon resonances in the $J^P = \frac{1}{2}^+$ and $\frac{3}{2}^+$ partial waves have been discussed in [59]. For convenience of the reader, we recall the main features here.

Above the Roper resonance, we observe a pole, given as $(\text{Re}(\text{pole}), -2\text{Im}(\text{pole}))$, at $(1690^{+25}_{-10}, 210 \pm 25)$ MeV or $(1695 \pm 15, 220 \pm 30)$ MeV for BG2010-01 and BG2010-02, respectively, which we identify with the known 3-star $N(1710)P_{11}$. A second resonance is seen at $(1860 \pm 20, 110^{+30}_{-10})$ MeV or $(1850^{+20}_{-50}, 360 \pm 40)$ MeV, respectively, with a width which depends sensitively on the solution. We call this resonance $N_{1/2^+}(1875)$ (this is the Breit-Wigner mass). A further pole at $(2100, 500)$ MeV improves the stability of the fit. The pole is also reported by KH84 [60] and CM [61]. We do neither claim its existence nor rule it out.

The $I(J^P) = \frac{1}{2}(\frac{3}{2})^+$ -wave houses, of course, the well known $N(1720)P_{13}$. Its pole position is determined to $(1695 \pm 30, 400 \pm 60)$ MeV or $(1670 \pm 30, 420 \pm 60)$ MeV, respectively. Above, there is at least one additional resonance $N(1900)P_{13}$ [42]; however, a better fit is obtained when a two-pole structure is assumed. In [59], we gave effective masses for the two resonances. The effective mass and the effective width are defined by the maximum and the full width at half maximum of the $\pi N \rightarrow MB$ transition strength where B, M stand for the final-state baryon and meson. These effective values are more stable against variations in the parameterization than Breit-Wigner parameters: the widths of resonances often become very large when three-body final states are included. We find, as mean value from a few transition amplitudes to different final states, $(M_{\text{eff}}, \Gamma_{\text{eff}}) = (1910 \pm 25, 300 \pm 70)$ and $(1970 \pm 20, 220 \pm 60)$ MeV for two resonances in the P_{13} wave. The two resonances differ in the photo-coupling; their decay modes were rather similar. Hence doubts remain in the existence of the upper resonance, in spite of the gain in χ^2 when it is introduced. Future experiments will have to decide if the splitting into two resonances is real. The existence of $N(1900)P_{13}$ with $(M_{\text{eff}}, \Gamma_{\text{eff}}) = (1910 \pm 25, 300 \pm 80)$ is, however, mandatory to achieve an acceptable fit.

3.1.2 $I(J^P) = \frac{1}{2}(\frac{5}{2})^+$

The lowest $I(J^P) = \frac{1}{2}(\frac{5}{2})^+$ state, $N(1680)F_{15}$, is well established and its properties, including photoproduction couplings, are known with a good precision. Real and imaginary part of the amplitude derived from energy independent analysis [62] are shown in Fig. 7a,b. The amplitude exhibits a beautiful resonance behavior due to $N(1680)F_{15}$. We reproduce the resonance with properties fully consistent with those given in [69].

The situation at higher masses is, however, far from being satisfactory. A rather narrow state, with the mass 1882 ± 10

and width 95 ± 20 , was observed in the KH84 analysis of the elastic πN data [60]. This state was confirmed by SAID [62], although with a notably lower mass (1818 MeV). In contrary, an observation of a rather broad state ($M = 1903 \pm 87, \Gamma = 490 \pm 310$ MeV) was reported from the combined analysis of the πN elastic data and $\pi N \rightarrow 2\pi N$ data [80]. The state was not observed in the CM analysis [61].

In [60,62], the evidence for this second F_{15} state is derived from the small structure in the amplitude (Fig. 7) at about 1.9 GeV which is present in the amplitudes from KH and GWU. Including a second resonance in the F_{15} wave, the KH points were described with a good χ^2 , the GWU points with a fair χ^2 .

Our coupled-channel analysis demands a second $5/2^+$ state in the region above 1800 MeV even though at a considerably higher mass. In a two-pole five-channel K-matrix parameterization of the F_{15} partial wave, the position of the second pole was found to be at $2050 \pm 30 - i235 \pm 20$ (see Table 1). The elastic πN amplitude is described with a modest $\chi^2/N_{\text{data}} = 4.72$ per data point (BG2011-02), see Fig. 7a,b. The solution BG2011-01 produces a similar description, with $\chi^2/N_{\text{data}} = 4.44$. Moreover we did not find a notable difference for the parameterization of this wave in our solutions BG2011-01 and BG2011-02.

The need for a second resonance above $N(1680)F_{15}$ can be visualized in a mass scan. Mass scans with two K-matrix poles are difficult to interpret, hence the F_{15} partial wave is parameterized as a sum of a one-pole K-matrix and a Breit-Wigner amplitude. With this parameterization we performed a mass scan where the mass of the Breit-Wigner amplitude was varied in defined steps, while all other parameters of the fit were allowed to re-adjust in each step. The χ^2 of the fit is thus a function of the assumed Breit-Wigner mass. The need for a further F_{15} resonance above $N(1680)F_{15}$ can also be seen, e.g., from two fits - with one and with two F_{15} resonances, respectively - shown in Fig. 6.

Fig. 8a shows the χ^2 as a function of the assumed Breit-Wigner mass in the $I(J^P) = 1/2(5/2^+)$ partial wave. A clear minimum in χ^2 is observed at about 2100 MeV. Main χ^2 changes stem from deteriorations of the fit to the differential cross section and the recoil polarization for $\gamma p \rightarrow K^+ \Lambda$ and of $\pi^- p \rightarrow K^0 \Lambda$ (Fig. 8b,c). In the former reaction, the χ^2 changes in the double polarization variables C_x, C_z, O_x, O_z are small, below 20 units, and are not included in the plot. The minimum in all distributions is well defined, although it is slightly lower in mass for the photoproduction data than for pion induced reactions.

The structure in the F_{15} amplitude at about 1.9 GeV (Fig. 7a,b) is not well described in the fit with two K-matrix poles. Hence we introduced a three-pole five-channel K-matrix to describe the F_{15} partial wave and increased the weight of the F_{15} elastic amplitude points in the fit. The new solutions reproduce the SAID F_{15} amplitude with $\chi^2/N_{\text{data}} = 1.82$ (BG2011-01) and $\chi^2/N_{\text{data}} = 1.91$ (BG2011-02): see Fig. 7c,d. For the KH amplitude, the χ^2/N_{data} improved from 3.75 for the two-pole solution BG2011-02 to 0.73 for the three-pole solution BG2011-02: see Fig. 7e,f. The total χ^2 improved by 750 units, mostly due to improvements in the description of elastic F_{15} amplitude (320) and the $\gamma p \rightarrow \pi^0 p$ data (400). However, we found two types of the three-pole solutions:

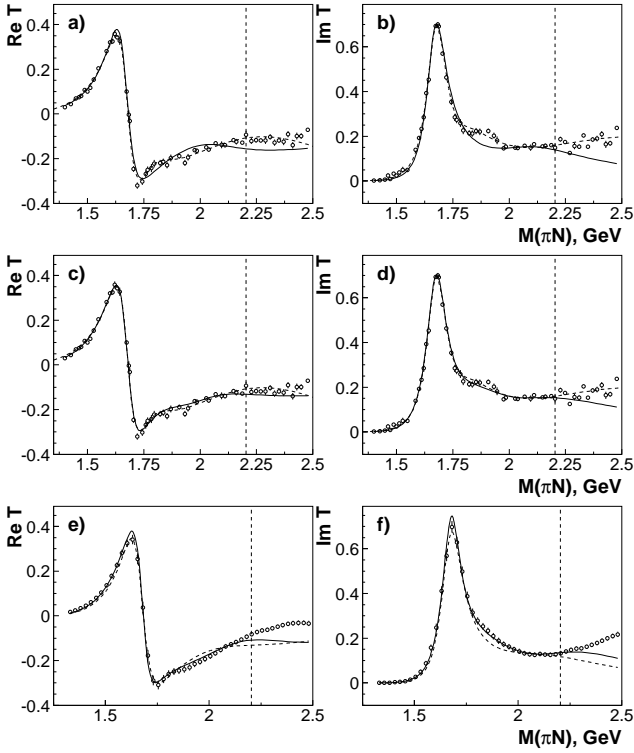


Fig. 7. Real and imaginary part of the $\frac{1}{2}(\frac{5}{2})^+$ partial wave amplitude. Points with error bars are from SAID energy independent solution [62] (a-d) and from KH84 [60] (f,e). The KH84 errors are assumed to be $\pm 5\%$. (a,b) SAID energy dependent fit (dashed curves) and fit BG2011-02 with two poles (solid curves). (c,d) SAID fit (dashed curves) and fit BG2011-02 with three poles (solid curves). (e,f) Fit BG2011-02 with two poles (dashed curves) and three poles (solid curves). Points in the high-mass region, defined by the vertical dashed line, were not included in the fit.

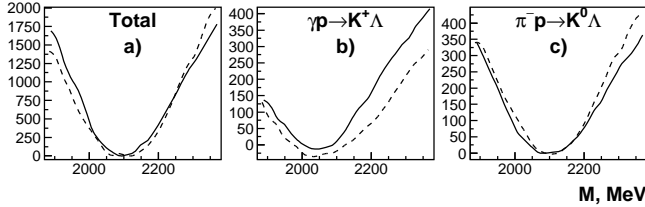


Fig. 8. Mass scan in the F_{15} wave above $N(1680)F_{15}$: a) the change of total χ^2 , b) the change of χ^2 value for the description of the $\gamma p \rightarrow K\Lambda$ data, differential cross section and recoil polarization, and c) the change of χ^2 for the description of the $\pi^- p \rightarrow K\Lambda$ data. The solution BG2011-02 is shown with solid curves and the solution BG2011-01 with dashed curves.

In the solution (a), the second pole is located in the mass region 1800–1950 MeV and its imaginary part corresponds to a width of 120 – 300 MeV. This pole has not only a high inelasticity; more than 80% of its decays must go into channels like ρN and ωN since nearly no evidence is seen for this resonance in the channels studied here (except $\gamma N, \pi N \rightarrow \pi N$). The third pole in this solution is shifted to a higher mass, by about 50 MeV. The third pole for this solution is given in Table 1 while the second pole is not, since its mass is ill defined.

Table 1. F_{15} wave: Pole positions and residues of the transition amplitudes (given in MeV as $|r|/\Theta$ with $Res A = |r| e^{i\Theta}$). The phases are given in degrees. The helicity couplings are given in $10^{-3} \text{ GeV}^{-1/2}$. The errors are defined from the spread of results found in the respective classes of solutions. The RPP values are given in parentheses. The third pole in the three-pole solution (a) is ill defined. It is located in the 1800–1950 MeV mass range.

Solution	2 poles	3 poles (Sol. a)
State	$N(2000)F_{15}$	$N(2000)F_{15}$
Re(pole)	2050 ± 30 (-)	2095^{+30}_{-60} (-)
-2Im(pole)	470 ± 40 (-)	500 ± 80 (-)
BW mass	2090 ± 20 (~ 2000)	2190 ± 40 (~ 2000)
BW width	450 ± 40 (-)	550 ± 100 (-)
$A(\pi N \rightarrow \pi N)$	$20 \pm 4 / -60 \pm 20^\circ$	$33 \pm 10 / -115 \pm 40^\circ$
$A(\pi N \rightarrow K\Lambda)$	$20 \pm 5 / 80 \pm 25^\circ$	$16 \pm 8 / 70 \pm 30^\circ$
$A(\pi N \rightarrow K\Sigma)$	$15 \pm 5 / 70 \pm 25^\circ$	$5 \pm 3 / -$
$A^{1/2}(\gamma p)$	$42 \pm 5 / -30 \pm 10^\circ$	$35 \pm 20 / 20 \pm 20^\circ$
$A^{3/2}(\gamma p)$	$48 \pm 5 / -170 \pm 25^\circ$	$50 \pm 20 / -130 \pm 35^\circ$
Solution	3 poles (Sol. b)	3 poles (Sol. b)
State	$N_{5/2}^+(1900)$	$N(2000)F_{15}$
Re(pole)	1930 ± 70 (-)	1920 ± 70
-2Im(pole)	400 ± 40 (-)	540 ± 40
BW mass	2000 ± 50 (~ 2000)	2000 ± 50
BW width	410 ± 40 (-)	500 ± 40
$A(\pi N \rightarrow \pi N)$	$70 \pm 20 / -100 \pm 80^\circ$	$140 \pm 25 / -80 \pm 40^\circ$
$A^{1/2}(\gamma p)$	$50 \pm 15 / 150 \pm 40^\circ$	$45 \pm 10 / 55 \pm 40^\circ$
$A^{3/2}(\gamma p)$	$65 \pm 10 / -15 \pm 40^\circ$	$75 \pm 15 / -110 \pm 40^\circ$

In solutions of type (b), the two highest poles come very close to each other; both are located in the 1900–1980 MeV region, and in the complex plane one pole falls atop of the other one. The pole position and couplings for these solutions are listed in Table 1. If both poles correspond to real resonances, one of the poles must have large couplings to ρN and ωN while the other couples significantly to $K\Lambda$.

In all solutions, using the SAID [62] or KH84 [60] F_{15} amplitude, a two-pole or three-pole K-matrix, one pole is required in the 1950–2100 mass region. It leads to a highly significant χ^2 improvement in reactions with $K\Lambda$ in the final state. There is suggestive evidence for a further pole between 1800 and 1950 MeV: this state is mainly needed to improve the description of the elastic amplitudes. Its existence is supported by the analyses of Höhler [62], of Manley *et al.* [80], and, based on our analysis, its existence seems rather likely. We do not claim that this state must exist but we certainly cannot rule out the possibility that it does exist. In the discussion, we refer to this state as $N_{5/2}^+(1875)$.

In Fig. 1e,f we show the contribution of the $\frac{1}{2}(\frac{5}{2})^+$ partial wave to the $\gamma p \rightarrow K^+\Lambda$ total cross section. The contribution is calculated starting from the three-pole solution (a) and using the SAID F_{15} πN amplitude [62].

In Table 1 we present details of the fits: pole position, Breit-Wigner parameters, residue of the elastic pole and helicity am-

plitudes. For this partial wave the solutions BG2011-01 and BG2011-02 produce very similar results; the small differences are included in the given errors.

3.1.3 $I(J^P) = \frac{1}{2}(\frac{7}{2}^+)$

Observations of a $\frac{1}{2}(\frac{7}{2})^+$ state in the 2 GeV mass region were reported from early KH84 [60] and CM [61] analyses of the πN elastic data, and from an analysis which included data on $\pi N \rightarrow \pi\pi N$ [80]. Breit-Wigner mass and width were determined to $M = 2005 \pm 150$ MeV, $\Gamma = 350 \pm 100$ in [60], to $M = 1970 \pm 50$ MeV, $\Gamma = 350 \pm 120$ in [61], and to $M = 2086 \pm 28$ MeV, $\Gamma = 535 \pm 120$ in [80]. The resonance is listed in RPP as $N(1990)F_{17}$. The resonance was not seen in the analysis presented in [62] (the $I(J^P) = \frac{1}{2}(\frac{7}{2})^+$ amplitude is not given in the paper but on their web site). Indeed, the $\frac{1}{2}(\frac{7}{2})^+$ amplitude (see Fig. 9) shows no significant structure.

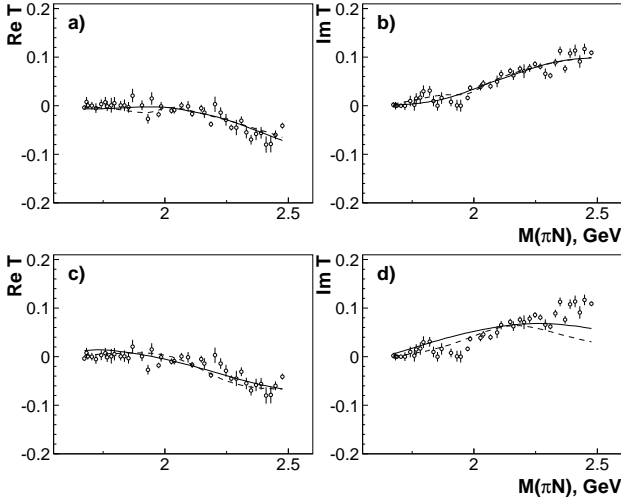


Fig. 9. Real and imaginary part of the $\frac{1}{2}(\frac{7}{2})^+$ partial wave. Points with error bars are from the SAID energy independent solution [62]. The solution BG2011-02 is shown as solid curve and BG2011-01 as dashed curve (a, b). Same solutions without a high mass pole (around 2400 MeV) (c, d).

The results of the SAID and KH84 energy independent partial wave analyses are shown in Fig. 9. A first attempt to describe this amplitude jointly with our full data base with a one-pole K-matrix parametrization failed. The main problem is that a rather narrow state around 2 GeV is required mainly by the data on $\gamma p \rightarrow K\Lambda$ and $\gamma p \rightarrow \pi^0 p$, which is incompatible with the πN elastic amplitude [62] in this partial wave. The description of the elastic amplitude improved considerably when a second K-matrix pole was included in the fit. Its mass is not well defined, any pole in the mass between 2300 and 2500 MeV is suited (Fig 9a,b).

The main improvements due to a F_{17} state are observed in the description of the recoil polarization in $\gamma p \rightarrow K\Lambda$. In this solution, the pole mass optimized for 1975 ± 15 MeV and the width for 160 ± 30 MeV. In the solution BG2011-2, mass and width were found to be 2100 ± 15 MeV and 260 ± 25 MeV.

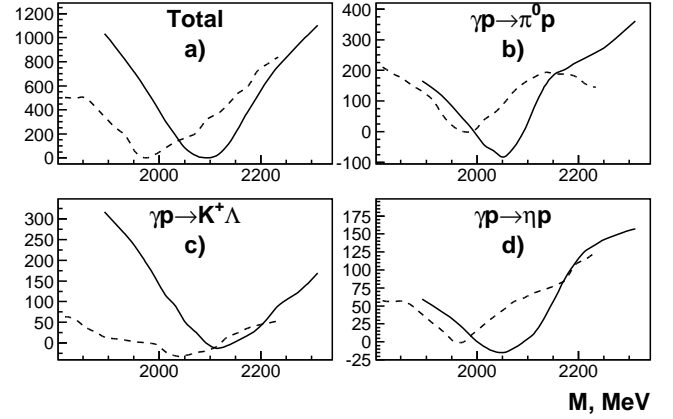


Fig. 10. Mass scan in the F_{17} wave with the BG2011-02 (solid line) and BG2011-01 (dashed line) solutions. a) Change of the total χ^2 , b) χ^2 change for $\gamma p \rightarrow \pi^0 p$, c) for $\gamma p \rightarrow K^+ \Lambda$, and d) for $\gamma p \rightarrow \eta p$.

Table 2. F_{17} wave: Pole positions and residues of the transition amplitudes (given in MeV as $|r|/\Theta$ with $ResA = |r|e^{i\Theta}$). The phases are given in degrees. The helicity couplings are given in $10^{-3}\text{GeV}^{-1/2}$. The errors are defined from the spread of results found in the respective classes of solutions.

Solution	BG2011-01	BG2011-02
State	$N(1990)F_{17}$	$N(1990)F_{17}$
Re(pole)	1975 ± 15	2100 ± 15
-2Im(pole)	160 ± 30	260 ± 25
BW mass	1990 ± 15	2105 ± 15
BW width	160 ± 30	260 ± 25
$A(\pi N \rightarrow \pi N)$	$1.5 \pm 0.5 / 180 \pm 30^\circ$	$1 \pm 0.5 / 80 \pm 20^\circ$
$A(\pi N \rightarrow K\Lambda)$	$1 \pm 1 / 170 \pm 30^\circ$	$0.5 \pm 0.5 / -100 \pm 30^\circ$
$A(\pi N \rightarrow K\Sigma)$	$1 \pm 0.5 / 100 \pm 30^\circ$	$0.3 \pm 0.3 / -60 \pm 40^\circ$
$A^{1/2}(\gamma p)$	$20 \pm 10 / 0 \pm 30^\circ$	$55 \pm 15 / -50 \pm 20^\circ$
$A^{3/2}(\gamma p)$	$35 \pm 10 / 0 \pm 20^\circ$	$55 \pm 20 / -50 \pm 25^\circ$

These two solutions have very different helicity couplings for the F_{17} state; therefore more precise polarization experiments should distinguish between them. Further studies revealed that in both classes of solutions, BG2011-01 and BG2011-02, a substitution of the whole F_{17} partial wave from one solution to the other one led to a very similar fit quality. For simplicity, we associate the low-mass resonance with BG2011-01 and the high-mass resonance with BG2011-02.

A mass scan in the F_{17} wave for the two solutions is shown in Fig. 10. In solution BG2011-02, all three reactions, $\gamma p \rightarrow K\Lambda$, $\gamma p \rightarrow \pi^0 p$, and $\gamma p \rightarrow \eta p$ contribute to the signal; in solution BG2011-01, the mass scan shows significant minima for $p\pi^0$, $n\pi^+$, $n\eta$, and a small dip only for $K^+\Lambda$.

The overall description of the data and the fit quality of the elastic amplitudes hardly differ for our two solutions BG2011-01 and BG2011-02; but the F_{17} amplitudes have their lowest-mass pole at a rather different position, at $(1975 - i80)$ or $(2100 - i130)$ MeV, respectively.

Table 3. H_{19} wave: Pole positions and residues of the transition amplitudes (given in MeV as $|r|/\Theta$ with $ResA = |r|e^{i\Theta}$). The phases are given in degrees. The helicity couplings are given in $10^{-3}GeV^{-1/2}$. The errors are defined from the spread of results found in both classes of solutions. The RPP values are given in parentheses.

State	$N(2220)H_{19}$	
Re(pole)	2150 ± 35	(~ 2170)
-2Im(pole)	440 ± 40	(~ 480)
BW mass	2200 ± 50	(~ 2250)
BW width	480 ± 60	(~ 400)
$A(\pi N \rightarrow \pi N)$	$60 \pm 12 / -58 \pm 12^\circ$	
$A^{1/2}(\gamma p)$	< 10	
$A^{3/2}(\gamma p)$	< 10	

3.1.4 $I(J^P) = \frac{1}{2}(\frac{9}{2}^+)$

The state $N(2220)H_{19}$ was clearly seen in the analysis of the elastic data. We fitted these data as one-pole three-channel (πN , $\pi \Delta$ and ρN) K-matrix and included a $\pi N \rightarrow \pi N$ non-resonant term. In the fits to the SAID [62] points, the non-resonant term can be taken as a constant while the fit to the KH84 [60] data, a more complicated form (see section 2) was chosen. The description of the SAID and KA84 results is shown in Fig. 11. We did not find any appreciable contribution from the $N(2220)H_{19}$ to the photoproduction data. The helicity couplings were optimized at very small values and the quality of the description did not improved after including this resonance in the photoproduction data. The pole position and elastic residue for this state (averaged over two solutions BG2011-01 and BG2011-02) is given in Table 3.

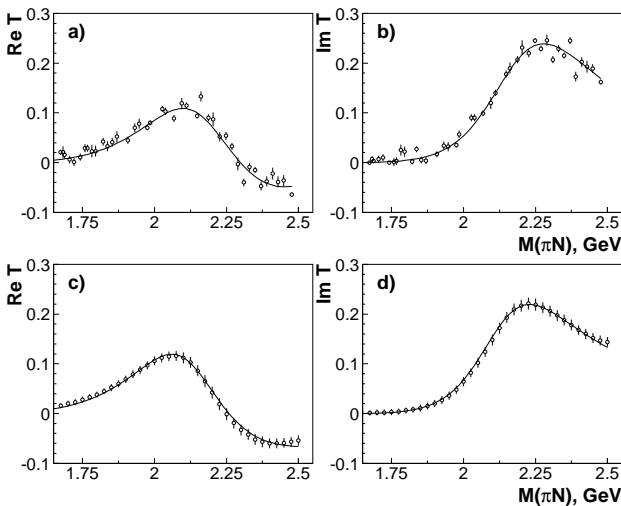


Fig. 11. Real and imaginary part of the $\frac{1}{2}(\frac{9}{2})^+$ partial wave. Points with error bars are from the SAID energy independent solution [62] (a,b) and from KH84 [60] (c,d). For KH84, $\pm 5\%$ errors were assumed.

3.2 Negative parity nucleon resonances

The mass spectrum of negative-parity nucleon resonances starts with the well known spin doublet $N(1535)S_{11}$, $N(1520)D_{13}$ in the second, and the spin triplet $N(1650)S_{11}$, $N(1700)D_{13}$, $N(1675)D_{15}$ in the third resonance region. Within SU(6), these states belong to a 70-plet. The next candidates listed in [69] are above 2 GeV and have only a RPP star rating of one or two stars. When we included the new CBELSA-TAPS data on $\gamma p \rightarrow K^0 \Sigma^+$, our fit failed to describe them with reasonable accuracy. We had to introduce two new negative parity resonances below 2 GeV (even though some evidence for both these resonances has been reported before). These two resonances also improved considerably our description of the new CLAS data on $\gamma p \rightarrow K^+ \Lambda$ [53]. We call these two states $N_{1/2-}(1895)$ and $N_{3/2-}(1875)$. A search for a resonance in the $(I)J^P = \frac{1}{2}(\frac{5}{2}^-)$ wave finds evidence at a considerably higher mass, at (2060 MeV). Our fits confirm the well-known $N(2190)G_{17}$ and $N(2250)G_{19}$ in the $(I)J^P = \frac{1}{2}(\frac{7}{2}^-)$ and $\frac{1}{2}(\frac{9}{2}^-)$ waves.

3.2.1 $I(J^P) = \frac{1}{2}(\frac{1}{2}^-)$

The first evidence for a rather narrow S_{11} state with the mass 1880 ± 20 and width 95 ± 30 MeV was reported by KH84 [60]. CM [61] observed a resonance, too, in this partial wave but at very different position: at $M = 2180 \pm 80$, $\Gamma = 350 \pm 100$ MeV. Manley *et al.* reported a low-mass state, but now with a broad width [80]. They reported $M = 1928 \pm 59$, $\Gamma = 414 \pm 157$ MeV. In the later analyses of the GWU group [62], there was no evidence at all for a third S_{11} state while Chen *et al.* [81] found positive evidence at 1878 MeV. These discrepant results are summarized by RPP under the one-star $N(2090)S_{11}$.

In the S_{11} partial wave, our fits required, in addition to the two-pole K-matrix parametrization of the low-energy part,

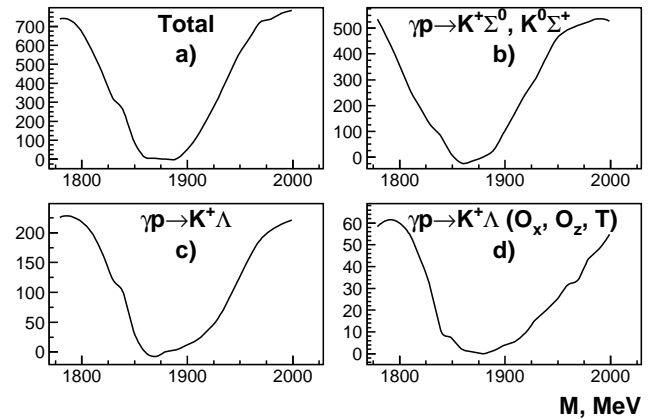


Fig. 12. Mass scan of a third S_{11} state. a) The change of total χ^2 , b) the change of χ^2 value for the description of the $\gamma p \rightarrow K^+ \Sigma^0, K^0 \Sigma^+$ differential cross section, c) the change of χ^2 for the description of the $\gamma p \rightarrow K^+ \Lambda$ differential cross section and d) change of χ^2 for the description of O_x, O_z and T observables in the $\gamma p \rightarrow K \Lambda$ reaction.

introduction of a further resonance at higher mass. A Breit-Wigner amplitude optimized at $M = 1895 \pm 15$, $\Gamma = 90^{+30}_{-15}$ MeV, in striking agreement with the result of the KH84 analysis. The resonance improved the description of differential cross section [53] and polarization observables O_x , O_z and T [50] from $\gamma p \rightarrow K^+ \Lambda$. For the latter data, a systematic improvement was obtained for two highest energy bins at 1883 and 1908 MeV. The mass scan of the S_{11} state for the solution BG2011-02 is shown in Fig. 12: it demonstrates a clear minimum for photoproduction of Λ and Σ hyperons, at the same mass and with a rather sharp minimum as expected for a narrow state.

To check whether the existence of $N_{1/2-}(1880)$ is in conflict with the elastic amplitudes extracted by the SAID and KA84 analyses we included this resonance as third K-matrix pole and refitted our full data base. The pole position of this state, found in the three-pole six-channel K-matrix fit πN , ηN , $K \Lambda$, $K \Sigma$, $\pi \Delta$ and ρN as well as elastic residues and photocoupling are given in Table. 4. The comparison of our elastic S_{11} amplitude with the SAID and KA84 energy fixed analysis is shown in Fig. 13.

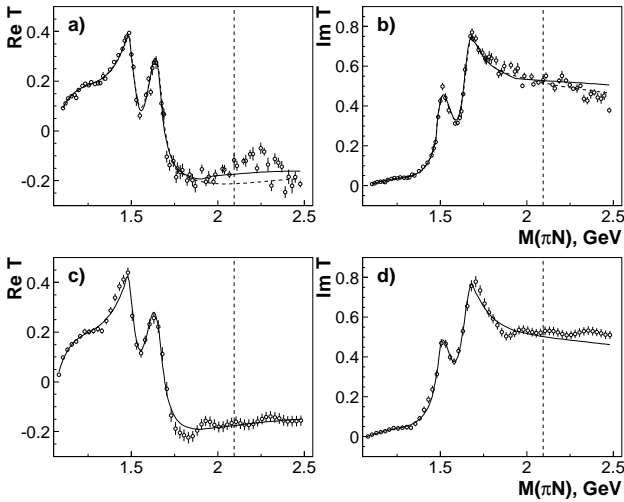


Fig. 13. Real and imaginary part of the $\frac{1}{2}(\frac{1}{2})^-$ partial wave. Points with error bars are from the SAID energy independent solution [62] (a,b) and from KH84 [60] (c,d). For KH84, $\pm 5\%$ errors were assumed. The SAID points are compared with our three pole (solid lines) and two pole solutions (dashed lines). The KH84 points are compared with three pole solution. Points in the high-mass region, defined by the vertical dashed line, were not included in the fit.

3.2.2 $I(J^P) = \frac{1}{2}(\frac{3}{2}^-)$

A resonance structure at about 1900 MeV in early SAPHIR data [82] was explained [83] by including a new resonance at 1895 MeV in the $I(J^P) = \frac{1}{2}(\frac{3}{2}^-)$ partial wave. Our first analysis of data on photoproduction of π^0 , η , and of Λ and Σ hyperons [39,40] suggested the existence of two resonances with masses above 1800 MeV in this wave which we called

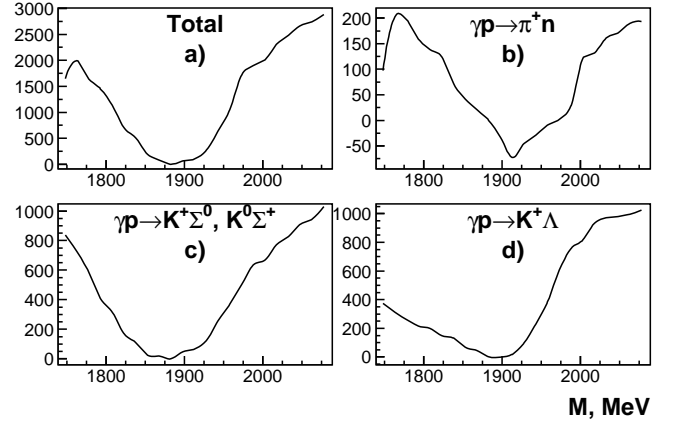


Fig. 14. The mass scan of the $D_{13}(1870)$ state. a) The change of total χ^2 , b) the change of χ^2 for the description of the $\gamma p \rightarrow \pi^+ n$ reactions, c) the change of χ^2 for the description of the $\gamma p \rightarrow K^+ \Sigma^0, K^0 \Sigma^+$ reactions and d) change of χ^2 for the description of the $\gamma p \rightarrow K^+ \Lambda$ reactions.

$N_{3/2-}(1875)$ and $N_{3/2-}(2170)$. The existence of the two resonances was required independently if the SAPHIR [84] or CLAS [48] data were used in the fit. The Breit-Wigner parameters of $D_{13}(1870)$ were found to be $M = 1875 \pm 25$ MeV and $\Gamma = 80 \pm 20$ MeV. The mass scan for this state had a clear minimum in the 1870-1880 MeV mass region, for $\gamma p \rightarrow \pi N$, $K^+ \Lambda$, and $K \Sigma$ [40].

The present analysis uses a significantly richer data base, and the parameters of these state are defined with a much better accuracy. In a first parameterization, the D_{13} partial wave was written as an amplitude K-matrix with two poles and non-resonant (contact) interactions; two Breit-Wigner amplitudes were added. The lower-mass Breit-Wigner resonance was found at 1880 ± 20 MeV and width at 200 ± 25 MeV. Its mass agrees precisely with our earlier finding, however the new data demand a notably larger width. The mass of the lower-mass Breit-Wigner amplitude was then scanned in a mass scan. The mass scan is shown in Fig. 14. It shows very clear minima for these reactions due to contributions from the new high statistic data [53,68,65,48].

Then, the D_{13} partial wave was written as an amplitude with three K-matrix poles, non-resonant (contact) interactions and one Breit-Wigner amplitude. The latter amplitude corresponded to the $D_{13}(2170)$ state. In [40], the high-mass state $D_{13}(2170)$ was found at $M = 2166^{+25}_{-50}$ MeV and $\Gamma = 300 \pm 65$ MeV. In the present analysis this state, we find its pole at $(2110 \pm 50) - i(170 \pm 23)$ MeV. The mass scan for this state is shown in Fig. 15: the most significant χ^2 are seen in the photoproduction of the $N\pi$ and $K^+ \Lambda$ final states.

Finally, a four-pole K-matrix was used. Pole positions, residues, and helicity amplitudes for both resonances are given in Table 4. A comparison of our elastic amplitude with the SAID and KA84 amplitudes is shown in Fig. 16. It is seen that in the fitted region our four-pole K-matrix describes these elastic amplitudes rather well. However our analysis suggest the possibility that at least one further D_{13} resonance at a higher mass might exist.

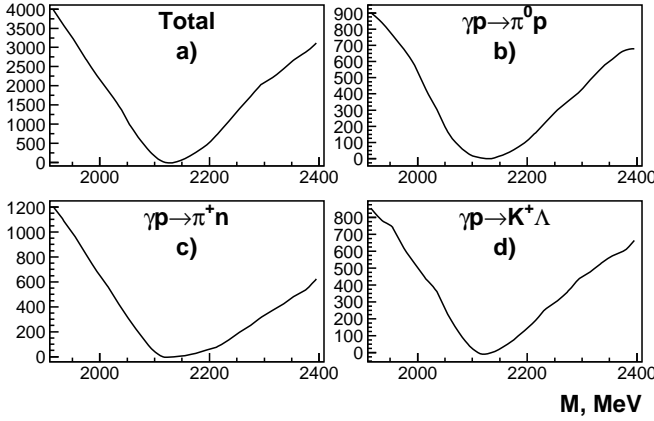


Fig. 15. The mass scan of the fourth D_{13} state. a) The change of total χ^2 , b) the change of χ^2 for the description of $\gamma p \rightarrow \pi^0 p$, c) of $\gamma p \rightarrow \pi^+ n$, and d) of χ^2 $\gamma p \rightarrow K^+ \Lambda$.

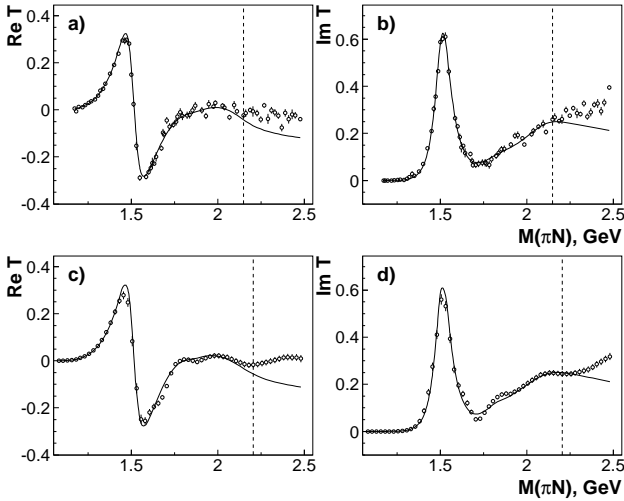


Fig. 16. Real and imaginary part of the $\frac{1}{2}(\frac{3}{2})^-$ partial wave. Points with error bars are from the SAID energy independent solution [62] (a,b) and from KH84 [60] (c,d). For KH84, $\pm 5\%$ errors were assumed. Points in the high-mass region, defined by the vertical dashed line, were not included in the fit.

3.2.3 $I(J^P) = \frac{1}{2}(\frac{5}{2}^-)$

The RPP [69] lists one high-mass resonance in the $I(J^P) = \frac{1}{2}(\frac{5}{2}^-)$ partial wave, the two-star $N(2200)D_{15}$. It was reported by [60] at $(M, \Gamma) = (2228 \pm 30, 310 \pm 50)$ MeV and by [61] at $(2180 \pm 80, 400 \pm 100)$ MeV. In our earlier analysis of the differential cross section on η photoproduction [63] we reported the observation of a new D_{15} resonance with a mass of about 2060 MeV. The state provided a dominant contribution to the $\gamma p \rightarrow \eta p$ cross section around 2050 MeV; possibly these observations are related. In the present solution, the contribution of this resonance to the $\gamma p \rightarrow \eta p$ cross section remains practically unchanged, but we find also a significant contribution from this state to $\gamma p \rightarrow K^+ \Lambda$. The new high statistic data on the differential cross section and recoil asymmetry [53] are much better described when this resonance is included. Also, the πN coupling of this state optimizes at a rather large value; it is of the

Table 4. Negative parity waves: Pole positions and residues of the transition amplitudes (given in MeV as $|r|/\Theta$ with $ResA = |r|e^{i\Theta}$). The phases are given in degrees. The helicity couplings are given in $10^{-3} GeV^{-1/2}$. BG2011-01 and BG2011-02 yield consistent results, the errors are hence defined from the spread of results found in the both classes of solutions. The RPP values are given in parentheses.

State	$N_{1/2-}(1895)$	$N_{3/2-}(1875)$
Re(pole)	1900 ± 15 (-)	1860 ± 25 (-)
-2Im(pole)	90^{+30}_{-15} (-)	200 ± 20 (-)
BW mass	1895 ± 15 (-)	1880 ± 20 (-)
BW width	90^{+30}_{-15} (-)	200 ± 25 (-)
$A(\pi N \rightarrow \pi N)$	0.5 ± 0.5 / -	2.5 ± 1 / -
$A(\pi N \rightarrow \eta N)$	2.5 ± 1.5 / $40 \pm 20^\circ$	
$A(\pi N \rightarrow K \Lambda)$	2 ± 1 / $90 \pm 30^\circ$	1.5 ± 1 / -
$A(\pi N \rightarrow K \Sigma)$	3 ± 2 / $40 \pm 30^\circ$	6 ± 2 / $180 \pm 50^\circ$
$A^{1/2}(\gamma p)$	12 ± 6 / $120 \pm 50^\circ$	18 ± 8 / $100 \pm 60^\circ$
$A^{3/2}(\gamma p)$		10 ± 4 / $180 \pm 30^\circ$
State	$N_{3/2-}(2150)$	$N_{5/2-}(2060)$
Re(pole)	2110 ± 50 (-)	2040 ± 15 (-)
-2Im(pole)	340 ± 45 (-)	390 ± 25 (-)
BW mass	2150 ± 60 (-)	2060 ± 15 (-)
BW width	330 ± 45 (-)	375 ± 25 (-)
$A(\pi N \rightarrow \pi N)$	13 ± 3 / $-20 \pm 10^\circ$	19 ± 5 / $-125 \pm 20^\circ$
$A(\pi N \rightarrow K \Lambda)$	5 ± 2 / $100 \pm 30^\circ$	1 ± 0.5 / $20 \pm 60^\circ$
$A(\pi N \rightarrow K \Sigma)$	3 ± 2 / $-50 \pm 40^\circ$	7 ± 4 / $-70 \pm 30^\circ$
$A^{1/2}(\gamma p)$	125 ± 45 / $-55 \pm 20^\circ$	65 ± 15 / $15 \pm 8^\circ$
$A^{3/2}(\gamma p)$	150 ± 60 / $-35 \pm 15^\circ$	55^{+15}_{-35} / $15 \pm 10^\circ$
State	$N(2190)G_{17}$	$N(2250)G_{19}$
Re(pole)	2150 ± 25 (~ 2075)	2195 ± 45 (~ 2200)
-2Im(pole)	330 ± 30 (~ 450)	470 ± 50 (~ 450)
BW mass	2180 ± 20 (~ 2190)	2280 ± 40 (~ 2275)
BW width	335 ± 40 (~ 500)	520 ± 50 (~ 500)
$A(\pi N \rightarrow \pi N)$	30 ± 5 / $30 \pm 10^\circ$	26 ± 5 / $-38 \pm 25^\circ$
$A(\pi N \rightarrow K \Lambda)$	4.5 ± 2 / $20 \pm 15^\circ$	
$A(\pi N \rightarrow K \Sigma)$	7 ± 3 / $90 \pm 30^\circ$	
$A^{1/2}(\gamma p)$	63 ± 7 / $-170 \pm 15^\circ$	< 10
$A^{3/2}(\gamma p)$	35 ± 20 / $25 \pm 10^\circ$	< 10

same order of magnitude as the ηN coupling constant. As a consequence, the mass scan of the $\frac{1}{2}(\frac{5}{2}^-)$ wave demonstrates very clear minima for the fit to $\gamma p \rightarrow \eta N$, to $\gamma p \rightarrow K^+ \Lambda$ and to both $\gamma p \rightarrow \pi N$ reactions (see Fig. 17).

The fit with the $N_{5/2-}(2060)$ state included as the second K-matrix pole reproduces perfectly the πN elastic amplitudes extracted by the SAID and KA84 groups: see Fig. 18. If the second pole is excluded from the fit, the high energy region can not be fitted well even after including energy dependent non-resonant terms. The problem of such a parameterization are demonstrated in Fig. 18. Although the elastic data indicate the existence of a resonance above 2 GeV, the pole position of this state is defined by the photoproduction data.

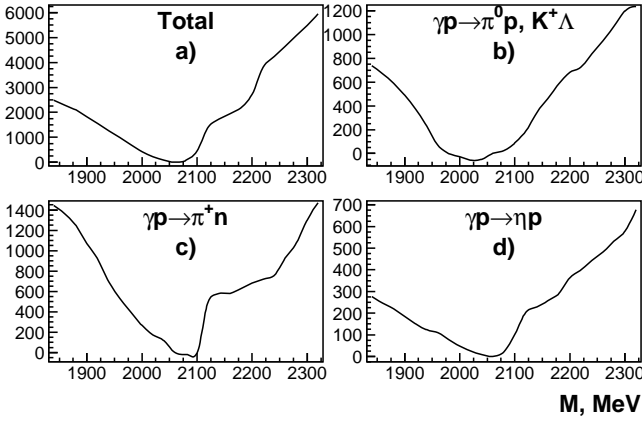


Fig. 17. The mass scan of the second D_{15} state. Changes of the χ^2 value: a) for all fitted data, b) for the $\gamma p \rightarrow \pi^0 p$ and $\gamma p \rightarrow K^+ \Lambda$ data, c) for the $\gamma p \rightarrow \pi^+ n$ differential cross section, d) for the $\gamma p \rightarrow \eta p$ differential cross section.

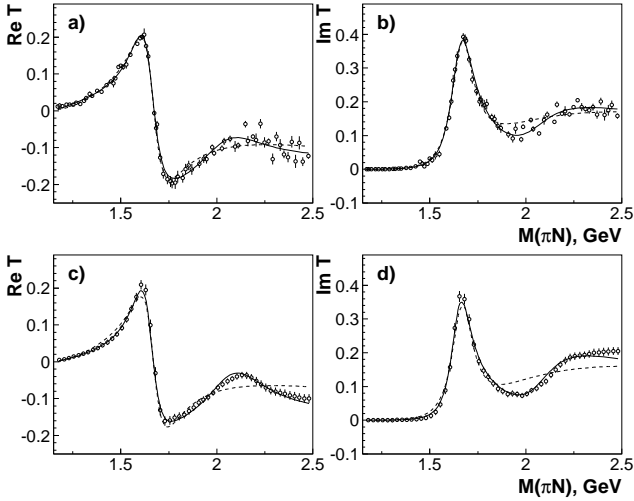


Fig. 18. Real and imaginary part of the $\frac{1}{2}(\frac{5}{2})^-$ partial wave. Points with error bars are from the SAID energy independent solution [62] (a,b) and from KH84 [60] (c,d). For KH84, $\pm 5\%$ errors were assumed. The solid curves show the result of two pole K-matrix parameterization and the dashed curves, the result of the one-pole parameterization from BG2011-02.

3.2.4 $I(J^P) = \frac{1}{2}(\frac{7}{2})^-$

A resonance in the $I(J^P) = \frac{1}{2}(\frac{7}{2})^-$ partial wave requires internal orbital angular momenta of $L = 3$; hence the lowest-mass resonance can be expected to have a mass of at least 2 GeV. Indeed, a resonance in this partial wave is clearly seen from the behavior of the elastic πN scattering amplitude. The amplitudes of the KH84 [60] and analyses [62] are shown in Fig. 19 as points with error bars. First, the real part crosses zero and the imaginary part reaches its maximum slightly above 2100 MeV, and second, the amplitude real part increases slowly starting from 1500 MeV indicating a broad structure. As the result, a one pole parameterization of the elastic amplitude [62] found a rather broad resonance with the mass 2152.4 ± 1.4 MeV and width 484 ± 13 MeV. Other analyses also found a resonance in

this region but with masses which cover the region 2100-2200 MeV and widths between 300 and 700 MeV (see references in RPP [69]).

An introduction of a $\frac{1}{2}(\frac{7}{2})^-$ state in the mass region 2100 MeV as a Breit-Wigner amplitude significantly improves the description of the $\gamma N \rightarrow K \Lambda$ differential cross section and recoil asymmetry [53]. Contributions of this partial wave to the $\gamma p \rightarrow K \Lambda$ total cross section are shown in Fig. 1. This state also contributed notably to the pion photoproduction. In our fits, the mass of the state was found to be compatible with the RPP numbers [69], the width was optimized slightly above 300 MeV. The fits required some contribution from non-resonant transitions (parameterized as constants) from $\gamma p \rightarrow \pi \Delta(1232)$ and ρN with the lowest orbital momentum.

The comparison of our πN elastic amplitude with the energy independent solution [62] is shown in Fig. 19. Our amplitude has a pole at $2150 - i 165$ MeV. This pole provides a good description of the $K \Lambda$ and πN photoproduction data and is compatible with the energy independent solution for the elastic amplitude [62] up to 2.4 GeV.

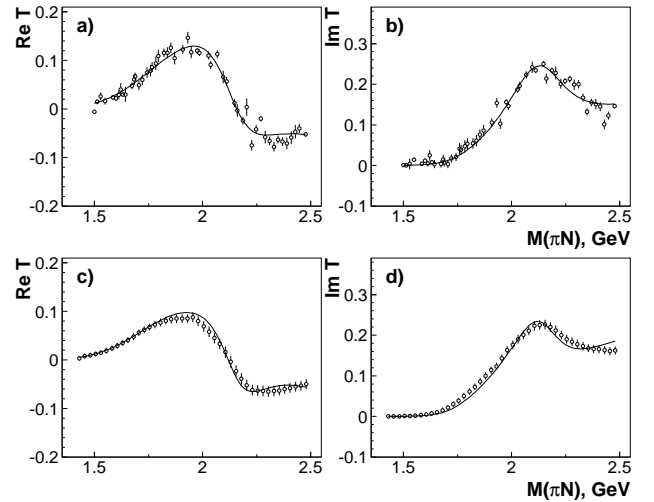


Fig. 19. Comparison of the result of energy independent analysis by SAID [62] (a, b) and KH84 [60] (c, d) for the $\frac{1}{2}(\frac{7}{2})^-$ partial wave with the BG2011-02 solution. For KH84, $\pm 5\%$ errors were assumed.

A mass scan in the $\frac{1}{2}(\frac{7}{2})^-$ wave shows very good minima for the total log likelihood value and for the sum of photoproduction contributions (see Fig. 20) while this state improves the description of the pion-induced inelastic reactions only marginally; the mass scan shows a small minimum for the solution BG2011-01 only.

3.2.5 $I(J^P) = \frac{1}{2}(\frac{9}{2})^-$

The state $N(2250)G_{19}$ has four stars by PDG classification and is clearly seen in the elastic data. As in the case of the $I(J^P) = 1/2(7/2^+)$ wave, the data were fitted as one-pole three-channel (πN , $\pi \Delta$ and ρN) K-matrix with a $\pi N \rightarrow \pi N$ non-resonant transition taken as a constant. The description of the SAID and

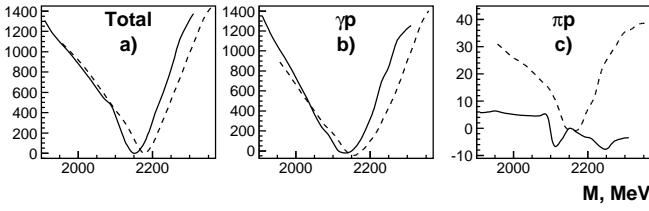


Fig. 20. Mass scan in the $\frac{1}{2}(\frac{7}{2})^-$ wave with the solution BG2011-02 (solid curves) and with the solution BG2011-01 (dashed curves). a) Change of the total χ^2 , b) change of the χ^2 value for all photoproduction reactions and c) change of the χ^2 value for all pion induced inelastic reactions.

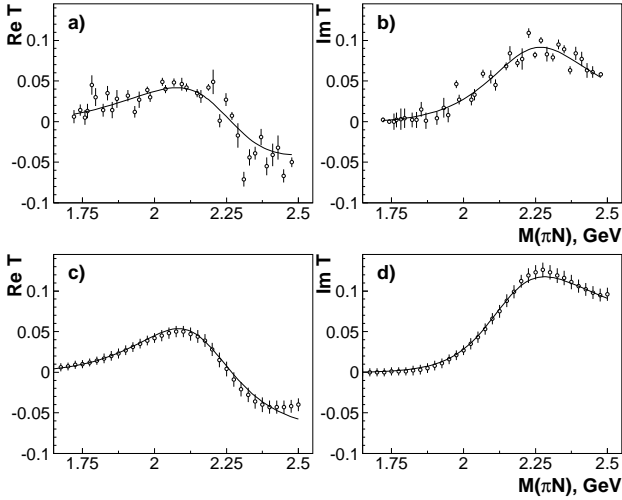


Fig. 21. Real and imaginary part of the $\frac{1}{2}(\frac{9}{2})^-$ partial wave. Points with error bars are from the SAID energy independent solution [62] (a,b) and from KH84 [60] (c,d). For KH84, $\pm 5\%$ errors were assumed.

KA84 results is shown in Fig. 21. The $N(2250)G_{19}$ state practically does not contribute to the photoproduction data and no additional sensitivity for this state was found when photoproduction data were included. The $K\Lambda$ coupling also optimized at a rather small value and this state contributed very little to the $\pi^- N \rightarrow K\Lambda$ data. Mass and width are given in Table 4.

4 Discussion and conclusions

4.1 Summary of nucleon resonances studied

Four resonances which we observe in our analysis are new in the sense that they have no defined entry in RPP [69]. We call them here $N_{1/2+}(1880)$, $N_{1/2-}(1895)$, $N_{3/2-}(1875)$, and $N_{5/2-}(2060)$. All four of them leave very significant traces in photoproduction, in particular in the reaction $\gamma p \rightarrow K^+\Lambda$. Here, we would like to remind the reader that nearly complete information exists on this reaction: The differential cross sections are known with high precision, the Λ recoil polarization is determined from its $N\pi$ weak decay, the beam asymmetry has been measured. Using linearly and circularly polarized photons, the polarization transfer coefficients from the initial photon to the Λ hyperon in the final state has been determined.

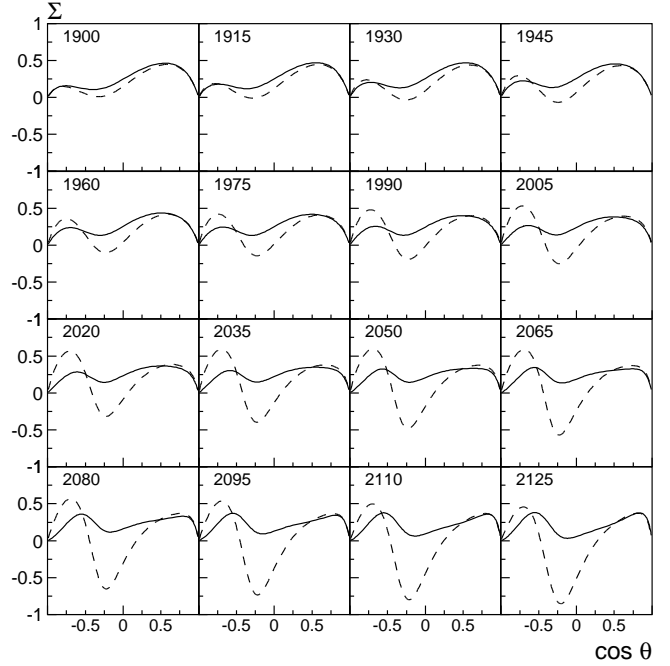


Fig. 22. Predictions of the beam asymmetry for the $\gamma p \rightarrow K^+\Lambda$ reaction. The full curve corresponds to the solution BG2011-02 and the dashed one corresponds to the solution BG2011-01.

From these quantities, the target asymmetry can be deduced algebraically. With one further measurement, e.g. the polarization correlation between target and Λ recoil polarization, the experimental information would be complete, in the sense that the results of all other polarization experiments can be predicted. Possibly, even a truly energy-independent reconstruction of the partial wave amplitudes will become possible.

In view of the excellent data base and the constraints provided by an energy dependent fit, we believe the solution(s) we present are highly constrained. To our judgement, the existence of these four resonances ranges from very likely to certain even though further information is desirable. At the same level we see the RPP resonances $N(1900)P_{13}$ and $N(2080)D_{13}$ - the latter resonance is observed at $M = 2150 \pm 60$, $\Gamma = 330 \pm 45$ MeV here. Based on pion-induced reactions, RPP classified them as two-star resonances [69].

The evidence for the existence of the two resonances in F -wave, the RPP states $N(2000)F_{15}$ and $N(1990)F_{17}$, is still only fair. We hope that forthcoming data with higher sensitivity will provide additional support for their existence and will define their properties with improved accuracy. In Fig. 22 and 23 we show the predicted beam asymmetry Σ and the double polarization variable F - the correlation between the degree of circular photon polarization and target polarization in the scattering plane and perpendicular to the photon beam - for $\gamma p \rightarrow K^+\Lambda$ for our two solutions BG2011-01 and BG2011-02. The figure may serve as an example that even a modest accuracy in polarization observables can make a significant impact on the results of a partial wave analysis.

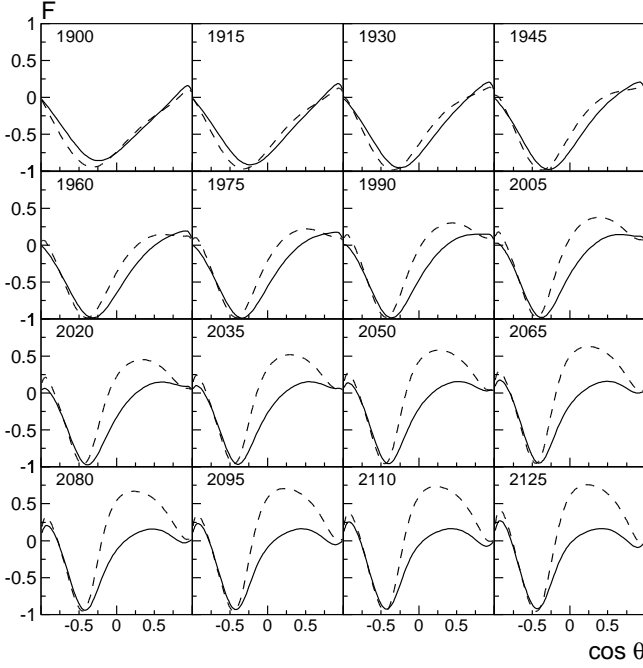


Fig. 23. Predictions of the double polarization variable F for the $\gamma p \rightarrow K^+ \Lambda$ reaction. The full curve corresponds to the solution BG2011-02 and the dashed one corresponds to the solution BG2011-01.

Table 5. Light-quark nucleon resonances. For resonances reported in this article we give our Breit-Wigner masses, for well known states we give nominal RPP masses, and for states reported in [59] we use names given there (M_{eff}). Mass values obtained from alternative solutions are given in a separate line.

$J =$	1/2	3/2	5/2	7/2	9/2
$N_{1/2+}$	(1710)				
		$N_{3/2+}$ (1720)	$N_{5/2+}$ (1680)		
$N_{1/2+}$	(1880)	$N_{3/2+}$ (1910)	$N_{5/2+}$ (2095)	$N_{7/2+}$ (2100)	
		alternatively: $\sim 1875 + 2200$		1990	
					$N_{9/2+}$ (2220)
$N_{1/2-}$	(1895)	$N_{3/2-}$ (1875)			
		$N_{3/2-}$ (2150)	$N_{5/2-}$ (2075)	$N_{7/2-}$ (2185)	$N_{9/2-}$ (2280)

4.2 Interpretation

For a discussion of the mass pattern of nucleon resonances, it is a bit tedious to refer to a resonance as $N(2200)D_{15}$ and to state: We, however, believe the mass of this resonance is rather 2075 MeV and not 2200 MeV. Hence we list in Table 5, with the mass we find, all positive-parity resonances in the 1650-2250 MeV mass range, and all negative-parity resonances in the 1750-2350 MeV mass range.

Two comments have to be made:

i) For the interpretation we use Breit-Wigner masses instead of pole positions. The reason is phenomenology. In lattice calculations and in quark models neglecting decays, the masses of isospin doublets like (ρ, ω) and $(a_1(1260), b_1(1235))$ are about mass degenerate. The pole masses are different - in particular for the $J^P = 1^+$ doublet with the very wide $a_1(1260)$

- while the Breit-Wigner masses are similar: The Breit-Wigner masses are closer to the bare poles of resonances; to the mass of resonances before they “dress themselves with a meson cloud”.

ii) The interpretations given below depend on the PWA solution. In a given interpretation, we chose the most appropriate pattern of resonances from Table 5. These alternatives can be decided as soon as new data can differentiate between the solutions presented above.

4.2.1 Interpretation within the quark model

Within the quark model light-quark baryons are assigned to SU(6) multiplets. For this discussion, some well known SU(6) relations are needed which - for the convenience of the reader - are reproduced here. The symmetry group SU(3) of the three flavors and the spin symmetry group SU(2) combine to the group SU(6) which decomposes according to

$$6 \otimes 6 \otimes 6 = 70_M + 70_M + 56_S + 20_A \quad (1)$$

where the subscript denotes the symmetry behavior with respect to the exchange of two quarks in the baryon. The baryon wave function can be symmetric (S), antisymmetric (A), or of mixed symmetry (M). These SU(6) groups can be written as sum of SU(3) groups with a defined spin multiplicity (given as superscript):

$$70 = {}^2 10 + {}^4 8 + {}^2 8 + {}^2 8 + {}^2 1 \quad (2)$$

$$56 = {}^4 10 + {}^2 8 \quad (3)$$

$$20 = {}^2 8 + {}^2 8 + {}^4 1 \quad (4)$$

The two resonances $N_{3/2+}(1720)$ and $N_{5/2+}(1680)$ are easily identified as spin doublet with intrinsic orbital and spin angular momenta $L = 2, S = 1/2$. Spin and flavor wave functions both have mixed symmetry, the spin-flavor wave function and the spatial wave function are likely symmetric. Hence they can be assigned to the $(D, L_N^P) = (56, 2_2^+)$ multiplet. Here, D is the dimensionality of the SU(6) multiplet, L^P intrinsic orbital angular momentum and the parity, N the shell number in the harmonic oscillator classification. The four states

$$N_{1/2+}(1880), N_{3/2+}(1910), N_{5/2+}(1875), N_{7/2+}(1990) \quad (5)$$

form a spin quartet which we assign to the $(D, L_N^P) = (70, 2_2^+)$ multiplet. Here, we have chosen the alternative mass values in Table 5 which are better adapted to the quark model. Missing is a spin doublet $(D, L_N^P) = (70, 2_2^+)$ with $J^P = \frac{3}{2}^+, \frac{5}{2}^+$.

Alternatively, we may assume that we have a spin-quartet of nucleon resonances

$$N_{1/2+}(2100), N_{3/2+}(1970), N_{5/2+}(2095), N_{7/2+}(2100) \quad (6)$$

and a spin-doublet

$$N_{1/2+}(1880), N_{3/2+}(1910). \quad (7)$$

The doublet should have $L = 1, S = 1/2$ and positive parity. Such a doublet is expected in quark models and assigned to a 20-plet in the SU(6) \times O(3) classification. This expectation is confirmed in recent lattice calculations [18]. The two

intrinsic oscillators both carry angular momentum $l_i = 1$, with $L = l_1 + l_2$: excitation of both oscillators is apparent.

Two positive-parity states, $N_{1/2+}(1440)$ and $N_{9/2+}(2220)$, remain to be discussed:

The Roper resonance $N_{1/2+}(1440)$ has been debated often; here we interpret it as nucleon radial excitation in the $(D, L_N^P) = (56, 0_2^+)$ multiplet. This interpretation does not exclude a sizeable molecular component in the wave function, in particular at small momentum transfer. The $N_{1/2+}(1710)$ resonance could belong to the $(D, L_N^P) = (70, 0_2^+)$ multiplet. In this interpretation we should expect an additional resonance with $J^P = \frac{3}{2}^+$. Finally, a further spin doublet is expected in quark models with $J^P = \frac{1}{2}^+, \frac{3}{2}^+$, where two internal quark angular momenta $l_i; i = 1, 2$ add to $L = 1$ and which would belong to the $(D, L_N^P) = (20, 1_2^+)$ multiplet.

$N_{9/2+}(2220)$ must have a minimum orbital angular momentum $L = 4$; its mass indicates where resonances in the fourth shell should be expected. It is hence assigned to the $(D, L_N^P) = (56, 4_4^+)$ multiplet.

The negative-parity nucleon resonances of Table 5 seem to be organized into a spin doublet

$$N_{1/2-}(1895), N_{3/2-}(1875) \quad (8)$$

with $L = 1$ and a spin quartet

$$N_{3/2-}(2150), N_{5/2-}(2075), N_{7/2-}(2190), N_{9/2-}(2250) \quad (9)$$

with $L = 3$. A spin doublet with $L = 1$ in a 70-plet should be accompanied by a spin triplet, i.e. at least a nucleon resonance with $J^P = \frac{5}{2}^-$ should exist at a close-by mass. $N_{5/2-}(2075)$ seems to be too high in mass and rather to belong to the spin-quartet. (The two additional resonances with $J^P = \frac{1}{2}^-$ and $J^P = \frac{3}{2}^-$ expected in addition to form a complete triplet could be hidden by a stronger production of the $N_{1/2-}(1895), N_{3/2-}(1875)$ spin doublet.) Hence we believe that $N_{1/2-}(1895), N_{3/2-}(1875)$ forms a spin doublet. As spin doublet without accompanying triplet it must belong to the $(D, L_N^P) = (56, 1_3^-)$ multiplet. Then the quartet (9) must belong to a $(D, L_N^P) = (70, 3_3^-)$ multiplet with a doublet with $J^P = \frac{5}{2}^-$ and $\frac{7}{2}^-$ missing. Possibly, they are unresolved parts of $N_{5/2-}(2075), N_{7/2-}(2190)$. With these assignments, six SU(6) multiplets are missing.

4.2.2 Interpretation within quark-diquark model

In the classical quark model, the three quarks obey the Pauli principle. In conventional diquark models it is assumed that two quarks – forming the diquark – are in relative S wave. Under these assumptions, the quartet of the states (5) in the mass region below 2 GeV is forbidden. However, when the wave function of the two quarks in the diquark and the single quark have no overlap, the Pauli principle should not be applied: far separated fermions do not obey the Pauli principle.

In [85] it is suggested that for highly excited states, the quark-diquark wave function and the quark wave function are spatially well separated. It is then an experimental question, which orbital angular momentum is required to satisfy the criterion of “full separation”. If for $L = 2$ the separation is

already sufficiently large, a quartet of states (5) is predicted in the region 1.9 GeV. At low energies, where the system is more compact and the quark-diquark wave functions overlap strongly, the baryon wave function obeys fully the Pauli principle and the additional states are suppressed.

4.2.3 Interpretation within AdS/QCD

AdS/QCD is an analytically solvable “gravitational” theory simulating QCD which is defined in a five-dimensional Anti-de Sitter (AdS) space embedded in six dimensions [86, 87, 88, 89]. In a special variant of AdS/QCD, a two-parameter mass formula was derived [33] which reproduces the baryon mass spectrum with a surprising precision. For the six rows in Table 5, the predicted masses are 1735, 1735, 1926, 2265, 1833, 2102 MeV, respectively. We mention that the mass formula had been suggested before on an empirical basis [32]. Again, the alternative solutions in Table 5 are preferred.

4.2.4 Interpretation as parity doublets

Table 5 exhibits a striking number of parity doublets. These are collected in Table 6. To the nucleons of the first line in Table 5 we have added the triplet of negative-parity resonances belonging to the first excitation band. The mass values of ambiguous solutions are chosen to match the masses of their negative-parity partners.

The occurrence of parity doublets in the mass spectrum of mesons and baryons is surprising. The harmonic oscillator states with positive and negative parity alternate, and in quark models, even in fully relativistic quark models, this pattern survives. In meson spectroscopy, a large number of resonances comes in nearly mass degenerate parity doublets, however with important exemptions: Mesons like $f_2(1270)$ and $a_2(1320)$ with $J^{PC} = 2^{++}$, $\omega_3(1670)$ and $\rho_3(1690)$ with $J^{PC} = 3^{--}$, $f_4(2050)$ and $a_4(2040)$ with $J^{PC} = 4^{++}$, none of these states falling onto the leading Regge trajectory has a mass-degenerate spin-parity partner. These are mesons in which the orbital angular momentum L and the total quark spin S are aligned to give the maximal J and which have the lowest mass in that partial wave. Their chiral partners have considerably higher masses: $\eta_2(1645)$ and $\pi_2(1670)$ ($J^{PC} = 2^{-+}$), $h_3(2045)$ and $b_3(2035)$ ($J^{PC} = 3^{+-}$), $\eta_4(2320)$ and $\pi_4(2250)$ ($J^{PC} = 4^{-+}$), respectively [90]. A graphical illustration is given in Fig. 1 of [91] and Fig. 57 of [92]. In [93] it is argued that formation

Table 6. Nucleon resonances as parity doublets. The masses of states for which ambiguous solutions exist are chosen to match their negative parity partners. Definition of masses as in Table 5.

$N_{1/2+}(1710)$	$N_{1/2-}(1650)$	$N_{3/2+}(1720)$	$N_{3/2-}(1700)$
$N_{5/2+}(1680)$	$N_{5/2-}(1675)$	$N_{1/2+}(1880)$	$N_{1/2-}(1895)$
$N_{3/2+}(1910)$	$N_{3/2-}(1875)$	$N_{5/2+}(2095)$	$N_{5/2-}(2075)$
$N_{7/2+}(2100)$	$N_{7/2-}(2190)$	$N_{9/2+}(2220)$	$N_{9/2-}(2250)$

of the spin-parity partners of mesons on the leading Regge trajectory could be suppressed by angular momentum barrier factors. A reanalysis of the reaction $\bar{p}p \rightarrow \pi\eta\eta$ in flight [94] was performed and a weak indication claimed [93] for the possible existence of the missing 4^{-+} state $\eta_4(1950)$ at about 1.95 GeV. However, the weakness of the signal is certainly not enforcing any interpretation. Nevertheless, the suppression in $\bar{p}p$ formation of spin-parity partners of mesons on the leading Regge trajectory is certainly an argument which reduces the weight of their non-observation.

In baryon spectroscopy, a similar phenomenon occurs. Even-parity resonances with $S = 3/2$ on a leading Regge trajectory seem to have no spin-parity partner [31]. In formation experiments, the same mechanism as in meson formation could possibly suppress these states. In elastic scattering, an angular momentum $L = 3$ is required to form a $7/2^{+}$ resonance; for $7/2^{-}$, $L = 4$ is needed. In photoproduction of baryon resonances, on the contrary, such a suppression is not expected. Baryons on the leading Regge trajectory, e.g. a $7/2^{+}$ resonance with the lowest mass, requires a E_4^{+} or M_4^{+} amplitude, a $7/2^{-}$ resonance a E_3^{-} or M_3^{-} amplitude. There is no kinematical factor which would suppress production of $7/2^{-}$ resonances compared to $7/2^{+}$ resonances. Photoproduction experiments could thus be of decisive importance to clarify the dynamics of highly excited hadrons. Unfortunately, the two solutions for the mass of the $5/2^{+}$ and $7/2^{+}$ resonances (listed in Table 5 prevent that a final decision can be made at present. Future experiments and analyses will be required. But the predictions in Fig. 22 and 23 show that a decision might be close.

4.3 Summary

In a multichannel partial wave analysis of nearly all existing data on pion- and photo-induced reactions we find evidence for a number of new or badly established resonances, and determine their properties. In particular, we observe four new resonances $N_{1/2^{+}}(1875)$, $N_{1/2^{-}}(1895)$, $N_{3/2^{-}}(1875)$ and $N_{5/2^{-}}(2075)$, and two resonances, $N(1900)P_{13}$ and $N(2080)D_{13}$ which were badly known so far. We believe that the existence of these three resonances is almost certain even though further confirmation is desirable. The new (and old) resonances are interpreted within different models.

Acknowledgements

We would like to thank the members of SFB/TR16 for continuous encouragement. We acknowledge support from the Deutsche Forschungsgemeinschaft (DFG) within the SFB/ TR16 and from the Forschungszentrum Jülich within the FFE program.

References

1. N. Isgur and G. Karl, Phys. Lett. B **72**, 109 (1977).
2. N. Isgur and G. Karl, Phys. Rev. D **18**, 4187 (1978).
3. N. Isgur and G. Karl, Phys. Rev. D **19**, 2653 (1979) [Erratum-ibid. D **23**, 817 (1981)].
4. S. Capstick and N. Isgur, Phys. Rev. D **34**, 2809 (1986).
5. U. Loring, B. C. Metsch and H. R. Petry, Eur. Phys. J. A **10**, 395 (2001).
6. L. Y. Glozman, W. Plessas, K. Varga and R. F. Wagenbrunn, Phys. Rev. D **58**, 094030 (1998).
7. S. Capstick and W. Roberts, Phys. Rev. D **47**, 1994 (1993).
8. S. Capstick and W. Roberts, Phys. Rev. D **49**, 4570 (1994).
9. S. Capstick and W. Roberts, Phys. Rev. D **58**, 074011 (1998).
10. T. Melde, W. Plessas and R. F. Wagenbrunn, Phys. Rev. C **72**, 015207 (2005) [Erratum-ibid. C **74**, 069901 (2006)].
11. S. Migura, D. Merten, B. Metsch and H. R. Petry, Eur. Phys. J. A **28**, 55 (2006).
12. S. Capstick, Phys. Rev. D **46**, 2864 (1992).
13. T. Van Cauteren, J. Ryckebusch, B. Metsch and H. R. Petry, Eur. Phys. J. A **26**, 339 (2005).
14. L. Y. Glozman, M. Radici, R. F. Wagenbrunn, S. Boffi, W. Klink and W. Plessas, Phys. Lett. B **516**, 183 (2001).
15. K. Berger, R. F. Wagenbrunn and W. Plessas, Phys. Rev. D **70**, 094027 (2004).
16. T. Van Cauteren, D. Merten, T. Corthals, S. Janssen, B. Metsch, H. R. Petry and J. Ryckebusch, Eur. Phys. J. A **20**, 283 (2004).
17. T. Melde, K. Berger, L. Canton, W. Plessas and R. F. Wagenbrunn, Phys. Rev. D **76** (2007) 074020.
18. R. G. Edwards, J. J. Dudek, D. G. Richards and S. J. Wallace, arXiv:1104.5152 [hep-ph].
19. A. J. G. Hey, R. L. Kelly, Phys. Rept. **96**, 71 (1983).
20. S. Capstick and W. Roberts, Prog. Part. Nucl. Phys. **45**, S241 (2000).
21. E. Klempt and J. M. Richard, Rev. Mod. Phys. **82** (2010) 1095.
22. O. Krehl, C. Hanhart, S. Krewald, and J. Speth, Phys. Rev. C **62**, 025207 (2000).
23. N. Kaiser, P. B. Siegel and W. Weise, Phys. Lett. B **362**, 23 (1995).
24. D. Jido, J. A. Oller, E. Oset, A. Ramos and U.-G. Meißner, Nucl. Phys. A **725**, 181 (2003)].
25. S. Capstick and P. R. Page, Phys. Rev. C **66**, 065204 (2002).
26. L. Y. Glozman, Phys. Lett. B **475**, 329 (2000).
27. R. L. Jaffe, Phys. Rept. **409**, 1 (2005) [Nucl. Phys. Proc. Suppl. **142**, 343 (2005)].
28. L. Y. Glozman, Phys. Rept. **444**, 1 (2007).
29. L. Y. Glozman and A. V. Nefediev, Nucl. Phys. A **807**, 38 (2008).
30. P. Bicudo, M. Cardoso, T. Van Cauteren and F. J. Llanes-Estrada, Phys. Rev. Lett. **103**, 092003 (2009).
31. E. Klempt, Phys. Lett. B **559**, 144 (2003).
32. E. Klempt, Phys. Rev. C **66**, 058201 (2002).
33. H. Forkel and E. Klempt, Phys. Lett. B **679**, 77 (2009).
34. See, e.g. S.J. Brodsky and F. Guy de Teramond, Chin. Phys. C **34**, 1 (2010).
35. A. Anisovich, E. Klempt, A. Sarantsev and U. Thoma, Eur. Phys. J. A **24**, 111 (2005).
36. E. Klempt, A. V. Anisovich, V. A. Nikonov, A. V. Sarantsev and U. Thoma, Eur. Phys. J. A **29** (2006) 307.
37. A. V. Anisovich and A. V. Sarantsev, Eur. Phys. J. A **30**, 427 (2006).
38. A. V. Anisovich, V. V. Anisovich, E. Klempt, V. A. Nikonov and A. V. Sarantsev, Eur. Phys. J. A **34** (2007) 129.
39. A. V. Anisovich, A. Sarantsev, O. Bartholomy, E. Klempt, V. A. Nikonov and U. Thoma, Eur. Phys. J. A **25**, 427 (2005).
40. A. V. Sarantsev, V. A. Nikonov, A. V. Anisovich, E. Klempt and U. Thoma, Eur. Phys. J. A **25**, 441 (2005).
41. A. V. Anisovich, V. Kleber, E. Klempt, V. A. Nikonov, A. V. Sarantsev and U. Thoma, Eur. Phys. J. A **34**, 243 (2007).
42. V. A. Nikonov, A. V. Anisovich, E. Klempt, A. V. Sarantsev and U. Thoma, Phys. Lett. B **662**, 245 (2008).

43. A. V. Anisovich, I. Jaegle, E. Klempt, B. Krusche, V. A. Nikonov, A. V. Sarantsev and U. Thoma, *Eur. Phys. J. A* **41**, 13 (2009).
44. A. V. Anisovich, E. Klempt, V. A. Nikonov, M. A. Matveev, A. V. Sarantsev and U. Thoma, *Eur. Phys. J. A* **44**, 203 (2010).
45. J. W. C. McNabb *et al.*, *Phys. Rev. C* **69**, 042201 (2004).
46. R. G. T. Zegers *et al.*, *Phys. Rev. Lett.* **91**, 092001 (2003).
47. R. Lawall *et al.*, *Eur. Phys. J. A* **24**, 275 (2005).
48. R. Bradford *et al.*, *Phys. Rev. C* **73**, 035202 (2006).
49. R. Bradford *et al.*, *Phys. Rev. C* **75**, 035205 (2007).
50. A. Lleres *et al.*, *Eur. Phys. J. A* **31**, 79 (2007).
51. R. Castelijns *et al.*, *Eur. Phys. J. A* **35**, 39 (2008).
52. A. Lleres *et al.*, *Eur. Phys. J. A* **39**, 149 (2009).
53. M. E. McCracken *et al.*, *Phys. Rev. C* **81**, 025201 (2010).
54. T. M. Knael *et al.*, *Phys. Rev. D* **11**, 1 (1975).
55. R. D. Baker *et al.*, *Nucl. Phys. B* **141**, 29 (1978).
56. D. H. Saxon *et al.*, *Nucl. Phys. B* **162**, 522 (1980).
57. J. C. Hart *et al.*, *Nucl. Phys. B* **166**, 73 (1980).
58. D. J. Candlin *et al.*, *Nucl. Phys. B* **226**, 1 (1983).
59. A. V. Anisovich, E. Klempt, V. A. Nikonov, A. V. Sarantsev, U. Thoma, *Eur. Phys. J. A* **47**, 27 (2011).
60. G. Höhler and H. Schopper, "Numerical Data And Functional Relationships In Science And Technology. Group I: Nuclear And Particle Physics. Vol. 9: Elastic And Charge Exchange Scattering Of Elementary Particles. B: Pion Nucleon Scattering. Pt. 2: Methods And R," *Berlin, Germany: Springer (1983) 601 P. (Landolt-Boernstein. New Series, I/9B2).*
61. R. E. Cutkosky, C. P. Forsyth, J. B. Babcock, R. L. Kelly and R. E. Hendrick, "Pion - Nucleon Partial Wave Analysis," 4th Int. Conf. on Baryon Resonances, Toronto, Canada, Jul 14-16, 1980. Published in *Baryon 1980:19 (QCD161:C45:1980)*
62. R. A. Arndt, W. J. Briscoe, I. I. Strakovsky and R. L. Workman, *Phys. Rev. C* **74**, 045205 (2006).
63. O. Bartholomy *et al.*, *Phys. Rev. Lett.* **94**, 012003 (2005).
64. H. van Pee *et al.*, *Eur. Phys. J. A* **31**, 61 (2007).
65. M. Dugger *et al.*, *Phys. Rev. C* **79**, 065206 (2009).
66. V. Crede *et al.*, *Phys. Rev. C* **80**, 055202 (2009).
67. B. Dey *et al.* [CLAS Collaboration], *Phys. Rev. C* **82** (2010) 025202.
68. R. Ewald *et al.* "Indication of a cusp-like structure in $K^0 \Sigma^+$ photoproduction off the proton", in preparation.
69. K. Nakamura *et al.* [Particle Data Group Collaboration], *J. Phys. G* **G37**, 075021 (2010).
70. M. Winik, S. Toaff, D. Revel, J. Goldberg and L. Berny, *Nucl. Phys. B* **128** (1977) 66.
71. F. S. Crawford, F. Grard and G. A. Smith, *Phys. Rev.* **128**, 368 (1962).
72. C. Baltay *et al.*, *Rev. Mod. Phys.* **33**, 374 (1961).
73. N. L. Carayannopoulos *et al.*, *Phys. Rev.* **138**, 433 (1965).
74. E. H. Bellamy *et al.*, *Phys. Lett. B* **39** (1972) 299.
75. E. F. McNicoll *et al.* [Crystal Ball Collaboration at MAMI], *Phys. Rev. C* **82** (2010) 035208.
76. J. Hartman. Talks given at the NSTAR 2011 (JLAB, Newport News, USA) and PWA 2011 (GWU, Washington, USA) workshops.
77. A. V. Anisovich, E. Klempt, V. Kuznetsov, V. A. Nikonov, M. V. Polyakov, A. V. Sarantsev, U. Thoma, [arXiv:1108.3010 [hep-ph]].
78. N. Sparks *et al.*, *Phys. Rev. C* **81**, 065210 (2010).
79. O. Bartalini *et al.* [The GRAAL Collaboration], *Eur. Phys. J. A* **A33**, 169-184 (2007). [arXiv:0707.1385 [nucl-ex]].
80. D. M. Manley and E. M. Saleski, *Phys. Rev. D* **45**, 4002 (1992).
81. G. Y. Chen, S. S. Kamalov, S. N. Yang, D. Drechsel and L. Tiator, *Phys. Rev. C* **76**, 035206 (2007) [arXiv:nucl-th/0703096].
82. M. Q. Tran *et al.* [SAPHIR Collaboration], *Phys. Lett. B* **445**, 20 (1998).
83. T. Mart, C. Bennhold, *Phys. Rev. C* **C61**, 012201 (2000).
84. K. H. Glander *et al.*, *Eur. Phys. J. A* **19**, 251 (2004).
85. A. V. Anisovich, V. V. Anisovich, M. A. Matveev, V. A. Nikonov, A. V. Sarantsev and T. O. Vulf, *Int. J. Mod. Phys. A* **25** (2010) 2965 [Int. J. Mod. Phys. A **25** (2010) 3155] [arXiv:1001.1259 [hep-ph]].
86. G. F. de Teramond and S. J. Brodsky, *Phys. Rev. Lett.* **94**, 201601 (2005).
87. A. Karch, E. Katz, D. T. Son and M. A. Stephanov, *Phys. Rev. D* **74** (2006) 015005.
88. H. Forkel, M. Beyer and T. Frederico, *JHEP* **0707**, 077 (2007).
89. For a survey on light-front dynamics and AdS/QCD, see S. J. Brodsky and G. de Teramond, arXiv:1010.4962 [hep-th], and references therein.
90. D. V. Bugg, *Phys. Rept.* **397**, 257 (2004).
91. S.S. Afonin, *Eur. Phys. J. A* **29**, 327 (2006).
92. E. Klempt and A. Zaitsev, *Phys. Rept.* **454**, 1 (2007).
93. L.Y. Glozman and A. Sarantsev, *Phys. Rev. D* **82**, 037501 (2010).
94. A.V. Anisovich *et al.*, *Phys. Lett. B* **491**, 47 (2000).

